Available online at www.sciencedirect.com
SCIENCE DIRECT®
Journal of Computational Physics 205 (2005) 72–97
JOURNAL OF COMPUTATIONAL PHYSICS
www.elsevier.com/locate/jcp

Local discontinuous Galerkin methods for nonlinear Schrödinger equations

Yan Xu [a], Chi-Wang Shu [b,*]

[a] Department of Mathematics, University of Science and Technology of China, Hefei, Anhui 230026, PR China
[b] Division of Applied Mathematics, Brown University, Box F, Providence, RI 02912, USA

Received 21 July 2004; received in revised form 1 November 2004; accepted 1 November 2004
Available online 9 December 2004

Abstract

In this paper we develop a local discontinuous Galerkin method to solve the generalized nonlinear Schrödinger equation and the coupled nonlinear Schrödinger equation. L^2 stability of the schemes are obtained for both of these nonlinear equations. Numerical examples are shown to demonstrate the accuracy and capability of these methods.

MSC: 65M60; 35Q55
Keywords: Local discontinuous Galerkin method; Nonlinear Schrödinger equation

1. Introduction

In this paper we develop a local discontinuous Galerkin method to solve the generalized nonlinear Schrödinger (NLS) equation

$$\mathrm{i}u_t + u_{xx} + \mathrm{i}(g(|u|^2)u)_x + f(|u|^2)u = 0, \tag{1.1}$$

the two-dimensional version

$$\mathrm{i}u_t + \Delta u + f(|u|^2)u = 0, \tag{1.2}$$

and the coupled nonlinear Schrödinger equation

* Corresponding author. Tel.: +1 401 863 2549; fax: +1 401 863 1355.
E-mail addresses: yxu1@mail.ustc.edu.cn (Y. Xu), shu@dam.brown.edu (C.-W. Shu).

0021-9991/$ - see front matter
doi:10.1016/j.jcp.2004.11.001

$$\begin{cases} iu_t + i\alpha u_x + u_{xx} + \beta u + \kappa v + f(|u|^2, |v|^2)u = 0, \\ iv_t - i\alpha v_x + v_{xx} - \beta u + \kappa v + g(|u|^2, |v|^2)v = 0, \end{cases} \tag{1.3}$$

where $f(u)$ and $g(u)$ are arbitrary (smooth) nonlinear real functions and α, β, κ are real constants.

The cubic nonlinear Schrödinger equation

$$iu_t + u_{xx} + |u|^2 u = 0, \tag{1.4}$$

which is a special case of Eq. (1.1), describes many phenomena and has important applications in fluid dynamics, nonlinear optics, and plasma physics [3,4,15]. Its structure is reminiscent of the Schrödinger equation in quantum physics, where $|u|^2$ has the significance of a potential. In Eq. (1.4) the complex function $u(x,t)$ describes the evolution of slowly varying wave trains in a stable dispersive physical system with no dissipation, for example waves in deep water. Various kinds of numerical methods can be found for simulating solutions of the NLS problems [5,17,20,21,24,25,29]. In [5,29], several important finite difference schemes are tested, analyzed and compared. In [24], a pseudospectral solution of GNLS equation is considered. A numerical solution of the NLS equation is obtained by using the quadratic B-spline finite element method in [17]. The convergence of a class of space–time finite element method for the nonlinear (cubic) Schrödinger equation is analyzed in [20,21]. The discontinuous Galerkin method considered in [20] refers to a discontinuous Galerkin discretization in time, hence is different from our approach of using a local discontinuous Galerkin discretization for the spatial variables.

The two-dimensional nonlinear Schrödinger equation (1.2) is a generic model for the slowly varying envelop of a wave-train in conservative, dispersive, mildly nonlinear wave phenomena. It is also obtained as the subsonic limit of the Zakharov model for Langmuir waves in plasma physics [34]. It is possible for solutions of the two-dimensional nonlinear Schrödinger equation to develop singularities at some finite time t_0 [18]. The linearized Crank–Nicolson finite difference scheme was used to compute the two-dimensional NLS equation in [27].

The coupled nonlinear Schrödinger equation

$$\begin{cases} iu_t + i\alpha u_x + \frac{1}{2}u_{xx} + (|u|^2 + \beta|v|^2)u = 0, \\ iv_t - i\alpha v_x + \frac{1}{2}v_{xx} + (\beta|u|^2 + |v|^2)v = 0, \end{cases} \tag{1.5}$$

were first derived 30 years ago by Benney and Newell [2] for two interacting nonlinear packets in a dispersive and conservative system. The classification of the solitary waves is considered in [33]. Ismail and Taha [19] introduced a finite difference method for the numerical simulation of the coupled nonlinear Schrödinger equation. In [28], a multi-symplectic formulation is considered.

The discontinuous Galerkin (DG) method we discuss in this paper is a class of finite element methods using a completely discontinuous piecewise polynomial space for the numerical solution and the test functions in the spatial variables, coupled with explicit and nonlinearly stable high order Runge–Kutta time discretization [26]. It was first developed for hyperbolic conservation laws containing first derivatives by Cockburn et al. [11,10,8,12] in a series of papers. For a detailed description of the method as well as its implementation and applications, we refer the readers to the lecture notes [7], the survey paper [9], other papers in that Springer volume, and the review paper [14].

These discontinuous Galerkin methods were generalized to solve a convection diffusion equation (containing second derivatives) by Cockburn and Shu [13]. Their work was motivated by the successful numerical experiments of Bassi and Rebay [1] for the compressible Navier–Stokes equations. Later, Yan and Shu [31] developed a local discontinuous Galerkin method for a general KdV type equation containing third derivatives, and they generalized the local discontinuous Galerkin method to PDEs with fourth and fifth spatial derivatives in [32]. Levy, Shu and Yan [22] developed local discontinuous Galerkin methods for solving nonlinear dispersive equations that have compactly supported traveling wave solutions, the

so-called "compactons". Recently, Xu and Shu [30] further developed the local discontinuous Galerkin method to solve three classes of nonlinear wave equations formulated by the general $K\mathrm{d}V$-Burgers type equations, the general fifth-order $K\mathrm{d}V$ type equations and the fully nonlinear $K(n,n,n)$ equations.

These discontinuous Galerkin methods have several attractive properties. It can be easily designed for any order of accuracy. In fact, the order of accuracy can be locally determined in each cell, thus allowing for efficient p adaptivity. It can be used on arbitrary triangulations, even those with hanging nodes, thus allowing for efficient h adaptivity. The methods have excellent parallel efficiency. It is extremely local in data communications. The evolution of the solution in each cell needs to communicate only with the immediate neighbors, regardless of the order of accuracy. Finally, it has excellent provable nonlinear stability. One can prove a strong L^2 stability and a cell entropy inequality for the square entropy, for the general nonlinear cases, for any orders of accuracy on arbitrary triangulations in any space dimension, without the need for nonlinear limiters.

The paper is organized as follows. In Section 2, we present and analyze the local discontinuous Galerkin methods for the NLS equations. In Section 2.1, we present the methods for the generalized NLS equations. We prove a theoretical result of L^2 stability for the nonlinear case as well as an error estimate for the linear case. In Section 2.2, we present the local discontinuous Galerkin methods for the two-dimensional NLS equations and give a theoretical result of L^2 stability. In Section 2.3, we present a local discontinuous Galerkin method for the coupled NLS equations and give a theoretical result of L^2 stability. Section 3 contains numerical results for the nonlinear problems to demonstrate the accuracy and capability of the methods. Concluding remarks are given in Section 4.

2. The local discontinuous Galerkin methods for the NLS equations

2.1. A local discontinuous Galerkin method for the generalized NLS equation

In this section, we present and analyze a local discontinuous Galerkin method for the following nonlinear problem:

$$\mathrm{i}u_t + u_{xx} + \mathrm{i}(g(|u|^2)u)_x + f(|u|^2)u = 0, \tag{2.1}$$

with an initial condition

$$u(x,0) = u_0(x) \tag{2.2}$$

and periodic boundary conditions. Here $f(u)$ and $g(u)$ are arbitrary (smooth) nonlinear real functions. Notice that the assumption of periodic boundary conditions is for simplicity only and is not essential: the method as well as the analysis can be easily adapted for non-periodic boundary conditions.

We denote the mesh by $I_j = [x_{j-\frac{1}{2}}, x_{j+\frac{1}{2}}]$ for $j = 1,\ldots,N$. The center of the cell is $x_j = (x_{j-\frac{1}{2}} + x_{j+\frac{1}{2}})/2$ and $\Delta x_j = x_{j+\frac{1}{2}} - x_{j-\frac{1}{2}}$. We denote by $u^+_{j+\frac{1}{2}}$ and $u^-_{j+\frac{1}{2}}$ the value of u at $x_{j+\frac{1}{2}}$, from the right cell, I_{j+1}, and from the left cell, I_j, respectively. We define the complex piecewise-polynomial space $V_{\Delta x}$ as the space of polynomials of degree at most k in each cell I_j, i.e.

$$V_{\Delta x} = \{v : v \in P^k(I_j) \text{ for } x \in I_j,\ j = 1,\ldots,N\}.$$

To define the local discontinuous Galerkin method, we rewrite Eq. (2.1) as a first-order system:

$$\begin{aligned} &\mathrm{i}u_t + p_x + \mathrm{i}(g(|u|^2)u)_x + f(|u|^2)u = 0,\\ &p - u_x = 0. \end{aligned} \tag{2.3}$$

Now we can apply the local discontinuous Galerkin method to Eqs. (2.3), find $u,p \in V_{\Delta x}$, $\forall v,w \in V_{\Delta x}$,

$$
\begin{aligned}
&\mathrm{i}\int_{I_j} u_t v\,\mathrm{d}x - \int_{I_j} p v_x\,\mathrm{d}x + (\hat{p}v^-)_{j+\frac{1}{2}} - (\hat{p}v^+)_{j-\frac{1}{2}} - \mathrm{i}\int_{I_j} g(|u|^2)uv_x\,\mathrm{d}x \\
&+ \mathrm{i}(\widehat{gu}v^-)_{j+\frac{1}{2}} - \mathrm{i}(\widehat{gu}v^+)_{j-\frac{1}{2}} + \int_{I_j} f(|u|^2)uv\,\mathrm{d}x = 0, \\
&\int_{I_j} pw\,\mathrm{d}x + \int_{I_j} uw_x\,\mathrm{d}x - ((\hat{u}w^-)_{j+\frac{1}{2}} - (\hat{u}w^+)_{j-\frac{1}{2}}) = 0.
\end{aligned} \tag{2.4}
$$

The "hat" terms in (2.4) in the cell boundary terms for integration by parts are the so-called "numerical fluxes", which are single valued functions defined on the edges and should be designed based on different guiding principles for different PDEs to ensure stability. For example, upwinding should be used as a guideline for odd derivatives which correspond to waves, and eventual symmetric treatment, such as an alternating choice of the fluxes for a quantity and its derivative, should be used for even derivatives. It turns out that we can take the simple choices such that

$$
\begin{aligned}
&\hat{u} = u^-, \quad \hat{p} = p^+, \quad \widehat{gu} = \hat{g}(|u^-|^2, |u^+|^2)\tilde{u}, \\
&\tilde{u} = \theta u^{up} + (1-\theta)(u^+ + u^-)/2, \quad u^{up} = \begin{cases} u^- & \text{if } \hat{g} \geqslant 0, \\ u^+ & \text{if } \hat{g} < 0, \end{cases} \quad 0 \leqslant \theta \leqslant 1,
\end{aligned} \tag{2.5}
$$

where we have omitted the half-integer indices $j+\frac{1}{2}$ as all quantities in (2.5) are computed at the same points (i.e. the interfaces between the cells). $\hat{g}(a,b)$ is monotone flux, i.e. Lipschitz continuous in both arguments, consistent (i.e. $\hat{g}(a,a) = g(a)$), non-decreasing in the first argument and non-increasing in the second. Examples of monotone fluxes which are suitable for discontinuous Galerkin methods can be found in, e.g. [11]. We could for example use the simple Lax–Friedrichs flux

$$
\hat{g}(a,b) = \frac{1}{2}(g(a) + g(b) - \alpha(b-a)), \quad \alpha = \max_a |g'(a)|,
$$

where the maximum is taken over a relevant range of $|u|^2$. The algorithm is now well defined. This flux is used in the numerical experiments in next section and we choose $\theta = 0$.

We remark that the choice for the fluxes (2.5) is not unique. In fact the crucial part is taking $\hat{u}$ and $\hat{p}$ from opposite sides.

With such a choice of fluxes we can get the theoretical results of L^2 stability.

Proposition 2.1. (cell entropy inequality). *There exist numerical entropy fluxes $\hat{\Phi}_{j+\frac{1}{2}}$ such that the solution to the scheme (2.4) and (2.5) satisfies*

$$
\frac{\mathrm{d}}{\mathrm{d}t}\int_{I_j} |u|^2\,\mathrm{d}x + \hat{\Phi}_{j+\frac{1}{2}} - \hat{\Phi}_{j-\frac{1}{2}} \leqslant 0.
$$

Proof. First, we take the complex conjugate for every term in Eq. (2.4)

$$
\begin{aligned}
&-\mathrm{i}\int_{I_j} u_t^* v^*\,\mathrm{d}x - \int_{I_j} p^* v_x^*\,\mathrm{d}x + (\hat{p}^* v^{*^-})_{j+\frac{1}{2}} - (\hat{p}^* v^{*^+})_{j-\frac{1}{2}} + \mathrm{i}\int_{I_j} g(|u|^2)u^* v_x^*\,\mathrm{d}x - \mathrm{i}(\widehat{gu^*}v^{*^-})_{j+\frac{1}{2}} + \mathrm{i}(\widehat{gu^*}v^{*^+})_{j-\frac{1}{2}} \\
&+ \int_{I_j} f(|u|^2)u^* v^*\,\mathrm{d}x = 0, \\
&\int_{I_j} p^* w^*\,\mathrm{d}x + \int_{I_j} u^* w_x^*\,\mathrm{d}x - ((\widehat{u^* w^{*^-}})_{j+\frac{1}{2}} - (\widehat{u^* w^{*^+}})_{j-\frac{1}{2}}) = 0,
\end{aligned} \tag{2.6}
$$

where u^* denote the the complex conjugate. Since (2.4) and (2.6) hold for any test functions in $V_{\Delta x}$, we can choose

$$v = u^*, \quad w = p^*.$$

With these choices of test functions and taking the difference of the sum of the two equalities in (2.4) and the sum of the two equalities in (2.6), we can get

$$\begin{aligned} &\mathrm{i}\int_{I_j}(|u|^2)_t\,\mathrm{d}x - \int_{I_j}(pu^*)_x\,\mathrm{d}x + ((\hat{p}u^{*^-} + \widehat{u^*}p^-)_{j+\frac{1}{2}} - (\hat{p}u^{*^+} + \widehat{u^*}p^+)_{j-\frac{1}{2}}) + \int_{I_j}(p^*u)_x\,\mathrm{d}x - ((\hat{u}p^{*^-} + \widehat{p^*}u^-)_{j+\frac{1}{2}} \\ &- (\hat{u}p^{*^+} + \widehat{p^*}u^+)_{j-\frac{1}{2}}) - \mathrm{i}\int_{I_j} g(|u|^2)(|u|^2)_x\,\mathrm{d}x + \mathrm{i}(\widehat{gu}u^{*^-} + \widehat{gu^*}u^-)_{j+\frac{1}{2}} - \mathrm{i}(\widehat{gu}u^{*^+} + \widehat{gu^*}u^+)_{j-\frac{1}{2}} \\ &= 0. \end{aligned}$$

Take $G(\tau) = \int^\tau g(\tau)\mathrm{d}\tau$, with definition (2.5) of the numerical fluxes and after some algebraic manipulation, we have

$$\int_{I_j}(|u|^2)_t\,\mathrm{d}x + \hat{\Phi}_{j+\frac{1}{2}} - \hat{\Phi}_{j-\frac{1}{2}} + \Theta_{j-\frac{1}{2}} = 0,$$

where the numerical entropy flux is given by

$$\hat{\Phi} = 2\,\mathrm{Im}(u^{*^-}p^+) - G(|u^-|^2) + \widehat{gu}u^{*^-} + \widehat{gu^*}u^-$$

and the extra term Θ is given by

$$\begin{aligned} \Theta &= [G(|u|^2)] - (\widehat{gu}[u^*] + \widehat{gu^*}[u]) \\ &= \int_{|u^-|^2}^{|u^+|^2}(g(\tau) - \hat{g}(|u^-|^2, |u^+|^2))\mathrm{d}\tau + \theta\hat{g}(|u^-|^2, |u^+|^2)((u^+ - u^{up})[u^*] + ((u^-)^* - (u^{up})^*)[u]) \geqslant 0, \end{aligned}$$

where $[u] \equiv u^+ - u^-$ denotes the jump of u, and we have used the monotonicity of $\hat{g}$ as well as the definition of the upwind value u^{up} to reach the last inequality. Now we have

$$\int_{I_j}(|u|^2)_t\,\mathrm{d}x + \hat{\Phi}_{j+\frac{1}{2}} - \hat{\Phi}_{j-\frac{1}{2}} \leqslant 0.$$

This is the cell entropy inequality.

Summing up the cell entropy inequalities, we obtain

Corollary 2.2. (L^2 stability). *The solution to the scheme (2.4) and (2.5) satisfies the L^2 stability*

$$\frac{\mathrm{d}}{\mathrm{d}t}\int_0^L |u|^2\,\mathrm{d}x \leqslant 0.$$

For actual numerical implementation, it might be more efficient if we decompose the complex function $u(x,t)$ into its real and imaginary parts by writing

$$u(x,t) = r(x,t) + \mathrm{i}s(x,t), \tag{2.7}$$

where r and s are real functions. Under the new notation, the problem (2.1) can be written as

$$\begin{aligned} &r_t + s_{xx} + (g(r^2+s^2)r)_x + f(r^2+s^2)s = 0, \\ &s_t - r_{xx} + (g(r^2+s^2)s)_x - f(r^2+s^2)r = 0, \end{aligned} \tag{2.8}$$

which can also be written as an equivalent first-order system:

$$
\begin{aligned}
&r_t + p_x + (g(r^2+s^2)r)_x + f(r^2+s^2)s = 0,\\
&p - s_x = 0,\\
&s_t - q_x + (g(r^2+s^2)s)_x - f(r^2+s^2)r = 0,\\
&q - r_x = 0.
\end{aligned}
$$

The local discontinuous Galerkin method (2.4) then becomes: find $r,p,s,q \in V_{\Delta x}$, which now denotes real piecewise polynomial of degree at most k, such that $\forall v,w,z,h \in V_{\Delta x}$,

$$
\begin{aligned}
&\int_{I_j} r_t v\,\mathrm{d}x - \int_{I_j} p v_x\,\mathrm{d}x + (\hat{p}v^-)_{j+\frac{1}{2}} - (\hat{p}v^+)_{j-\frac{1}{2}} - \int_{I_j} g(s^2+r^2) r v_x\,\mathrm{d}x + (\widehat{gr}v^-)_{j+\frac{1}{2}} - (\widehat{gr}v^+)_{j-\frac{1}{2}}\\
&\quad + \int_{I_j} f(r^2+s^2) s v\,\mathrm{d}x = 0,\\
&\int_{I_j} p w\,\mathrm{d}x + \int_{I_j} s w_x\,\mathrm{d}x - (\hat{s}w^-)_{j+\frac{1}{2}} + (\hat{s}w^+)_{j-\frac{1}{2}} = 0,\\
&\int_{I_j} s_t z\,\mathrm{d}x + \int_{I_j} q z_x\,\mathrm{d}x - (\hat{q}z^-)_{j+\frac{1}{2}} + (\hat{q}z^+)_{j-\frac{1}{2}} - \int_{I_j} g(s^2+r^2) s z_x\,\mathrm{d}x + (\widehat{gs}z^-)_{j+\frac{1}{2}} - (\widehat{gs}z^+)_{j-\frac{1}{2}}\\
&\quad - \int_{I_j} f(r^2+s^2) r z\,\mathrm{d}x = 0,\\
&\int_{I_j} q h\,\mathrm{d}x + \int_{I_j} r h_x\,\mathrm{d}x - (\hat{r}h^-)_{j+\frac{1}{2}} + (\hat{r}h^+)_{j-\frac{1}{2}} = 0.
\end{aligned}
\tag{2.9}
$$

The numerical fluxes become

$$
\begin{aligned}
&\hat{p} = p^+, \quad \hat{r} = r^-, \quad \hat{q} = q^+, \quad \hat{s} = s^-,\\
&\widehat{gr} = \hat{g}((s^2+r^2)^-, (s^2+r^2)^+)\tilde{r}, \quad \widehat{gs} = \hat{g}((s^2+r^2)^-, (s^2+r^2)^+)\tilde{s},\\
&\tilde{r} = \theta r^{up} + (1-\theta)(r^+ + r^-)/2, \quad r^{up} = \begin{cases} r^- & \text{if } \hat{g} \geqslant 0,\\ r^+ & \text{if } \hat{g} < 0,\end{cases}\\
&\tilde{s} = \theta s^{up} + (1-\theta)(s^+ + s^-)/2, \quad s^{up} = \begin{cases} s^- & \text{if } \hat{g} \geqslant 0,\\ s^+ & \text{if } \hat{g} < 0,\end{cases} \quad 0 \leqslant \theta \leqslant 1,
\end{aligned}
\tag{2.10}
$$

where we have omitted the half-integer indices $j+\frac{1}{2}$ as all quantities in (2.10) are computed at the same points (i.e. the interfaces between the cells).

Next, we consider the error estimate for linearized NLS equation

$$
\mathrm{i}u^e_t + u^e_{xx} + \mathrm{i}u^e_x + u^e = 0, \tag{2.11}
$$

where we use u^e to denote the exact solution of Eq. (2.11). The corresponding equations in real functions are

$$
\begin{aligned}
&r^e_t + s^e_{xx} + r^e_x + s^e = 0,\\
&s^e_t - r^e_{xx} + s^e_x - r^e = 0,
\end{aligned}
\tag{2.12}
$$

with the equivalent first-order system:

$$
\begin{aligned}
&r^e_t + p^e_x + r^e_x + s^e = 0,\\
&p^e - s^e_x = 0,\\
&s^e_t - q^e_x + s^e_x - r^e = 0,\\
&q^e - r^e_x = 0.
\end{aligned}
$$

We define

$$\begin{aligned} B_j(r,p,s,q;v,w,z,h) \equiv & \int_{I_j} r_t v\,\mathrm{d}x + \int_{I_j} s_t z\,\mathrm{d}x + \int_{I_j} sv\,\mathrm{d}x + \int_{I_j} pw\,\mathrm{d}x - \int_{I_j} rz\,\mathrm{d}x + \int_{I_j} qh\,\mathrm{d}x - \int_{I_j} pv_x\,\mathrm{d}x \\ & + (\hat{p}v^-)_{j+\frac{1}{2}} - (\hat{p}v^+)_{j-\frac{1}{2}} - \int_{I_j} rv_x\,\mathrm{d}x + (\tilde{r}v^-)_{j+\frac{1}{2}} - (\tilde{r}v^+)_{j-\frac{1}{2}} + \int_{I_j} qz_x\,\mathrm{d}x - (\hat{q}z^-)_{j+\frac{1}{2}} \\ & + (\hat{q}z^+)_{j-\frac{1}{2}} - \int_{I_j} sz_x\,\mathrm{d}x + (\tilde{s}z^-)_{j+\frac{1}{2}} - (\tilde{s}z^+)_{j-\frac{1}{2}} + \int_{I_j} sw_x\,\mathrm{d}x - (\hat{s}w^-)_{j+\frac{1}{2}} + (\hat{s}w^+)_{j-\frac{1}{2}} \\ & + \int_{I_j} rh_x\,\mathrm{d}x - (\hat{r}h^-)_{j+\frac{1}{2}} + (\hat{r}h^+)_{j-\frac{1}{2}}, \end{aligned}$$

where the monotone fluxes simply become upwinding

$$\tilde{r} = r^-, \quad \tilde{s} = s^-.$$

The local discontinuous Galerkin method for Eq. (2.12) becomes: find $r,p,s,q \in V_{\Delta x}$ such that, $\forall v,w,z,h \in V_{\Delta x}$,

$$B_j(r,p,s,q;v,w,z,h) = 0.$$

We clearly also have

$$B_j(r^e,p^e,s^e,q^e;v,w,z,h) = 0,$$

and we can then obtain the error equation

$$B_j(r^e - r, p^e - p, s^e - s, q^e - q; v,w,z,h) = 0 \tag{2.13}$$

for all $v,w,z,h \in V_{\Delta x}$. Take

$$v = \mathscr{S}r^e - r, \quad w = \mathscr{P}q^e - q, \quad z = \mathscr{S}s^e - s, \quad h = p - \mathscr{P}p^e,$$

where $\mathscr{P}$ is the standard L^2 projection into $V_{\Delta x}$, that is, for each j,

$$\int_{I_j} (\mathscr{P}w(x) - w(x))v(x)\,\mathrm{d}x = 0 \quad \forall v \in P^k,$$

and $\mathscr{S}$ is special projection into $V_{\Delta x}$ which satisfies, for each j,

$$\int_{I_j} (\mathscr{S}w(x) - w(x))v(x)\,\mathrm{d}x = 0 \ \ \forall v \in P^{k-1} \quad \text{and} \quad \mathscr{S}w(x^-_{j+\frac{1}{2}}) = w(x^-_{j+\frac{1}{2}}).$$

Then we have

$$B_j(v,-h,z,w;v,w,z,h) = B_j(v^e,-h^e,z^e,w^e;v,w,z,h), \tag{2.14}$$

where

$$v^e = \mathscr{S}r^e - r^e, \quad w^e = \mathscr{P}q^e - q^e, \quad z^e = \mathscr{S}s^e - s^e, \quad h^e = p^e - \mathscr{P}p^e.$$

By the same argument as that used for the cell entropy inequality, the left-hand side of (2.14) becomes

$$B_j(v,-h,z,w;v,w,z,h) = \int_{I_j} (v_t v + z_t z)\mathrm{d}x + \hat{\Phi}_{j+\frac{1}{2}} - \hat{\Phi}_{j-\frac{1}{2}} + \Theta_{j-\frac{1}{2}},$$

where

$$\hat{\Phi} = -h^+v^- - w^+z^- + \frac{1}{2}(v^2)^- + \frac{1}{2}(z^2)^-, \quad \Theta = \frac{1}{2}([v]^2 + [z]^2).$$

As to the right-hand side of (2.14), we have

$$B_j(v^e, -h^e, z^e, w^e; v, w, z, h) = I + II + III + IV,$$

where

$$I = \int_{I_j} (v_t^e v + z_t^e z)\mathrm{d}x,$$

$$II = \int_{I_j} ((w^e - z^e)z_x + (h^e - v^e)v_x + z^e w_x + v^e h_x - h^e w + w^e h + z^e v - v^e z)\mathrm{d}x,$$

$$III = (((h^e)^+ - (v^e)^-)[v] + ((w^e)^+ - (z^e)^-)[z] + (z^e)^-[w] + (v^e)^-[h])_{j-\frac{1}{2}},$$

and

$$IV = \hat{H}_{i+\frac{1}{2}} - \hat{H}_{i-\frac{1}{2}}$$

with

$$\hat{H} = -((h^e)^+ - (v^e)^-)v^- - ((w^e)^+ - (z^e)^-)z^- - (z^e)^- w^- - (v^e)^- h^-.$$

By using the simple inequality $ab \leqslant (\varepsilon/2)a^2 + (1/2\varepsilon)b^2$, and standard approximation theory [6] on $v_t^e = (\mathscr{S}r^e - r^e)_t$ and $z_t^e = (\mathscr{S}z^e - z^e)_t$, we have

$$I \leqslant C\Delta x_j^{2k+3} + \frac{1}{4}\int_{I_j} (v^2 + z^2)\mathrm{d}x.$$

Because $\mathscr{P}$ is a local L^2 projection, and $\mathscr{S}$, even though not a local L^2 projection, does have the property that $\omega - \mathscr{S}\omega$ is locally orthogonal to all polynomials of degree up to $k-1$, all the terms in II except the last two terms are actually zero. We can get the estimates for the last two terms in II:

$$\int_{I_j} (z^e v - v^e z)\mathrm{d}x \leqslant C\Delta x_j^{2k+3} + \frac{1}{4}\int_{I_j} (v^2 + z^2)\mathrm{d}x.$$

The last two terms in III are zero, because of the special interpolating property of the projection $\mathscr{S}$. An application of the simple inequality $ab \leqslant \frac{1}{2}(a^2 + b^2)$ for the first two terms in III and the standard approximation theory on the point values of $v^e = \mathscr{S}r^e - r^e$, $w^e = \mathscr{P}q^e - q^e$, $z^e = \mathscr{S}s^e - s^e$, $h^e = p^e - \mathscr{P}p^e$ then gives

$$III \leqslant C(\Delta x_{j-1}^{2k+2} + \Delta x_j^{2k+2}) + \frac{1}{4}([v]^2 + [z]^2).$$

Finally, IV only contains flux difference terms which will vanish upon a summation in j.

Combining all these and summing over j we obtain the following inequality:

$$\frac{\mathrm{d}}{\mathrm{d}t}\int_0^L \frac{1}{2}(v^2 + z^2)\mathrm{d}x + \frac{1}{4}([v]^2 + [z]^2) \leqslant \Delta x^{2k+1} + \int_0^L \frac{1}{2}(v^2 + z^2)\mathrm{d}x.$$

An integration in t plus the standard approximation theory on $v^e = (\mathscr{S}r^e - r^e)$ and $z^e = (\mathscr{S}s^e - s^e)$ then gives the desired error estimates.

Proposition 2.3. (error estimate). *The error for the scheme (2.9) and (2.10) applied to the linearized NLS equation (2.12) satisfies*

$$\|u^e - u\|_0 \leqslant C\|u^e\|_{k+1}\Delta x^{k+\frac{1}{2}}, \tag{2.15}$$

where $\|\cdot\|_m$ is the standard Sobolev m norm and the constant C depends on the time t.

2.2. The local discontinuous Galerkin method for two-dimensional NLS equations

In this section, we present and analyze the local discontinuous Galerkin method for the two-dimensional NLS equations

$$\mathrm{i}u_t + \Delta u + f(|u|^2)u = 0, \quad 0 \leqslant x, y \leqslant L, \tag{2.16}$$

with an initial condition

$$u(x, y, 0) = u_0(x, y) \tag{2.17}$$

and periodic boundary conditions. Here, $f(u)$ is an arbitrary (smooth) nonlinear real function. Notice that the assumption of a box geometry and periodic boundary conditions is for simplicity only and is not essential: the method can be easily designed for arbitrary domain and non-periodic boundary conditions.

We assume that the domain Ω is polygonal and denote by $\mathscr{T}_{\Delta x}$ a triangulation of Ω. Here Δx measures the longest edge of all polyhedra in $\mathscr{T}_{\Delta x}$. We again denote the complex finite element space by

$$V_{\Delta x} = \{v : v \in P^k(K) \text{ for } \forall K \in \mathscr{T}_{\Delta x}\}.$$

To define the local discontinuous Galerkin method, we rewrite Eq. (2.16) as a first-order system:

$$\begin{aligned} &\mathrm{i}u_t + p_x + q_y + f(|u|^2)u = 0,\\ &p - u_x = 0,\\ &q - u_y = 0. \end{aligned} \tag{2.18}$$

Now we can define the local discontinuous Galerkin method to Eqs. (2.18): find $u, p, q \in V_{\Delta x}$, such that, $\forall v, w, z \in V_{\Delta x}$,

$$\begin{aligned} &\mathrm{i}\int_K u_t v \,\mathrm{d}x\,\mathrm{d}y - \int_K p v_x \,\mathrm{d}x\,\mathrm{d}y + \int_{\partial K} \widehat{p_{n_{x,K}}} v^{int_K} \,\mathrm{d}s - \int_K q v_y \,\mathrm{d}x\,\mathrm{d}y + \int_{\partial K} \widehat{q_{n_{y,K}}} v^{int_K} \,\mathrm{d}s + \int_K f(|u|^2)uv \,\mathrm{d}x\,\mathrm{d}y = 0,\\ &\int_K pw \,\mathrm{d}x\,\mathrm{d}y + \int_K u w_x \,\mathrm{d}x\,\mathrm{d}y - \int_{\partial K} \widehat{u_{n_{x,K}}} w^{int_K} \,\mathrm{d}s = 0,\\ &\int_K qz \,\mathrm{d}x\,\mathrm{d}y + \int_K u z_y \,\mathrm{d}x\,\mathrm{d}y - \int_{\partial K} \widehat{u_{n_{y,K}}} z^{int_K} \,\mathrm{d}s = 0, \end{aligned} \tag{2.19}$$

where ∂K is the boundary of element K, and the numerical fluxes (the "hats") are defined similar to the one-dimensional cases, namely

$$\widehat{u_{n_{x,K}}} = u^- n_{x,K}, \quad \widehat{p_{n_{x,K}}} = p^+ n_{x,K}, \quad \widehat{u_{n_{y,K}}} = u^- n_{y,K}, \quad \widehat{q_{n_{y,K}}} = q^+ n_{y,K}, \tag{2.20}$$

where $(n_{x,K}, n_{y,K})$ are the outward unit normal for element K along the element boundary ∂K, u_K^{int} denotes the value of u evaluated from inside the element K, and v^-, v^+ refer to values of v at a uniquely defined "left" and "right" sides for each edge. For example, if all the elements K are rectangles, then on all horizontal edges, v^- denotes the value of v from below, and v^+ denotes the value of v from above; and on all vertical edges, v^- denotes the value of v from left, and v^+ denotes the value of v from right. The choice for the fluxes (2.20) is not unique. In fact the crucial part is taking $\widehat{u_{n_{x,K}}}$ and $\widehat{p_{n_{x,K}}}$, $\widehat{u_{n_{y,K}}}$ and $\widehat{q_{n_{y,K}}}$ from opposite sides.

With such a choice of fluxes we still have L^2 stability for the scheme (2.19) and (2.20). The proof follows the same lines as the one-dimensional case, so we omit it.

Proposition 2.4. (L^2 stability). *The solution to the scheme (2.19) and (2.20) satisfies the L^2 stability*

$$\frac{\mathrm{d}}{\mathrm{d}t}\int_\Omega |u|^2\,\mathrm{d}x\,\mathrm{d}y \leqslant 0.$$

2.3. The local discontinuous Galerkin method for coupled NLS equations

In this section, we present and analyze the local discontinuous Galerkin method for the coupled NLS equations

$$\begin{cases} \mathrm{i}u_t + \mathrm{i}\alpha u_x + u_{xx} + \beta u + \kappa v + f(|u|^2,|v|^2)u = 0, \\ \mathrm{i}v_t - \mathrm{i}\alpha v_x + v_{xx} - \beta u + \kappa v + g(|u|^2,|v|^2)v = 0, \end{cases} \tag{2.21}$$

with an initial condition

$$\begin{cases} u(x,0) = u_0(x), \\ v(x,0) = v_0(x), \end{cases} \tag{2.22}$$

and periodic boundary conditions. Here, $f(a,b)$ and $g(a,b)$ are arbitrary (smooth) nonlinear real functions, α,β,κ are constants. Notice again that the assumption of periodic boundary conditions is for simplicity only and is not essential: the method can be easily designed for non-periodic boundary conditions.

To define the local discontinuous Galerkin method, we rewrite Eq. (2.21) as a first-order system:

$$\begin{aligned} &\mathrm{i}u_t + \mathrm{i}\alpha u_x + p_x + \beta u + \kappa v + f(|u|^2,|v|^2)u = 0, \\ &p - u_x = 0, \\ &\mathrm{i}v_t - \mathrm{i}\alpha v_x + q_x - \beta u + \kappa v + g(|u|^2,|v|^2)v = 0, \\ &q - v_x = 0. \end{aligned} \tag{2.23}$$

Now we can define the local discontinuous Galerkin method to Eqs. (2.23): find $u,v,p,q \in V_{\Delta x}$, such that, $\forall r,w,s,z, \in V_{\Delta x}$,

$$\begin{aligned} &\mathrm{i}\int_{I_j} u_t r\,\mathrm{d}x - \mathrm{i}\alpha\int_{I_j} u r_x\,\mathrm{d}x + \mathrm{i}\alpha(\tilde{u}r^-)_{j+\frac{1}{2}} - \mathrm{i}\alpha(\tilde{u}r^+)_{j-\frac{1}{2}} - \int_{I_j} p r_x\,\mathrm{d}x + (\hat{p}r^-)_{j+\frac{1}{2}} - (\hat{p}r^+)_{j-\frac{1}{2}} \\ &\quad + \int_{I_j} (\beta u + \kappa v + f(|u|^2,|v|^2)u) r\,\mathrm{d}x = 0, \\ &\int_{I_j} p w\,\mathrm{d}x + \int_{I_j} u w_x\,\mathrm{d}x - ((\hat{u}w^-)_{j+\frac{1}{2}} - (\hat{u}w^+)_{j-\frac{1}{2}}) = 0, \\ &\mathrm{i}\int_{I_j} v_t s\,\mathrm{d}x + \mathrm{i}\alpha\int_{I_j} v s_x\,\mathrm{d}x - \mathrm{i}\alpha(\tilde{v}s^-)_{j+\frac{1}{2}} + \mathrm{i}\alpha(\tilde{v}s^+)_{j-\frac{1}{2}} - \int_{I_j} q s_x\,\mathrm{d}x + (\hat{q}s^-)_{j+\frac{1}{2}} - (\hat{q}s^+)_{j-\frac{1}{2}} \\ &\quad + \int_{I_j} (-\beta u + \kappa v + g(|u|^2,|v|^2)v) s\,\mathrm{d}x = 0 \\ &\int_{I_j} q z\,\mathrm{d}x + \int_{I_j} v z_x\,\mathrm{d}x - ((\hat{v}z^-)_{j+\frac{1}{2}} - (\hat{v}z^+)_{j-\frac{1}{2}}) = 0. \end{aligned} \tag{2.24}$$

The "hat" terms in (2.24) are again the numerical fluxes, which can be taken as

$$\begin{aligned} &\hat{u} = u^-, \quad \hat{p} = p^+, \quad \hat{v} = v^-, \quad \hat{q} = q^+, \\ &\tilde{u} = u^-, \quad \tilde{v} = v^+ \quad \text{if } \alpha > 0, \\ &\tilde{u} = u^+, \quad \tilde{v} = v^- \quad \text{if } \alpha < 0, \end{aligned} \tag{2.25}$$

where we have omitted the half-integer indices $j+\frac{1}{2}$ as all quantities in (2.25) are computed at the same points (i.e. the interfaces between the cells).

We remark that the choice for the fluxes (2.25) is not unique. In fact the crucial part is taking $\hat{u}$ and $\hat{p}$, $\hat{v}$ and $\hat{q}$ from opposite sides.

Table 1
Accuracy test for the NLS equation (3.1) with the plane wave solution (3.2)

	N	Real part				Imaginary part			
		L^2 error	Order	L^∞ error	Order	L^2 error	Order	L^∞ error	Order
p^0	20	6.92E − 02	–	1.82E − 01	–	6.98E − 02	–	1.83E − 01	–
	40	3.64E − 02	0.93	1.68E − 01	0.12	3.45E − 02	1.02	8.98E − 02	1.02
	80	1.73E − 02	1.08	7.34E − 02	1.19	1.70E − 02	1.02	4.34E − 02	1.05
	160	8.52E − 03	1.02	3.71E − 02	0.98	8.49E − 03	1.00	2.38E − 02	0.86
p^1	20	6.26E − 03	–	2.36E − 02	–	6.18E − 03	–	2.43E − 02	–
	40	1.59E − 03	1.98	6.21E − 03	1.93	1.66E − 03	1.90	1.14E − 02	1.09
	80	3.90E − 04	2.03	1.49E − 03	2.05	4.03E − 04	2.04	2.47E − 03	2.21
	160	9.87E − 05	1.98	3.73E − 04	2.00	9.92E − 05	2.02	5.95E − 04	2.05
p^2	20	1.24E − 04	–	6.56E − 04	–	1.32E − 04	–	6.27E − 04	–
	40	2.07E − 05	2.62	2.45E − 04	1.42	1.78E − 05	2.89	7.98E − 05	2.97
	80	2.17E − 06	3.26	2.62E − 05	3.22	1.94E − 06	3.20	1.01E − 05	2.99
	160	2.52E − 07	3.10	3.09E − 06	3.08	2.45E − 07	2.99	1.33E − 06	2.92
p^3	20	6.55E − 06	–	2.41E − 05	–	6.29E − 06	–	2.01E − 05	–
	40	4.61E − 07	3.83	1.59E − 06	3.93	5.37E − 07	3.55	4.04E − 06	2.31
	80	2.41E − 08	4.26	1.02E − 07	3.96	2.66E − 08	4.34	2.26E − 07	4.16
	160	1.50E − 09	4.01	5.52E − 09	4.20	1.53E − 09	4.12	1.37E − 08	4.05

$\alpha = 0.5$, $\beta = \gamma = 0$, $A = c = 1$. Periodic boundary condition in $[0, 2\pi]$. Non-uniform meshes with N cells at time $t = 1$.

Table 2
Accuracy test for the NLS equation (3.1) with the plane wave solution (3.2)

	N	Real part				Imaginary part			
		L^2 error	Order	L^∞ error	Order	L^2 error	Order	L^∞ error	Order
p^0	20	6.98E − 02	–	1.89E − 01	–	6.94E − 01	–	1.73E − 01	–
	40	3.62E − 02	0.95	9.32E − 02	1.02	3.68E − 02	0.91	1.38E − 01	0.33
	80	1.73E − 02	1.07	4.75E − 02	0.97	1.73E − 02	1.09	6.83E − 02	1.01
	160	8.58E − 03	1.01	2.21E − 02	1.10	8.59E − 03	1.01	3.20E − 02	1.09
p^1	20	1.61E − 02	–	3.28E − 02	–	1.62E − 02	–	3.12E − 02	–
	40	3.70E − 03	2.12	8.69E − 03	1.92	4.88E − 03	1.73	1.11E − 02	1.49
	80	9.58E − 04	1.95	1.93E − 03	2.17	1.03E − 03	2.25	2.21E − 03	2.33
	160	2.48E − 04	1.95	5.01E − 04	1.94	2.49E − 04	2.04	5.60E − 04	1.98
p^2	20	1.48E − 04	–	7.90E − 04	–	1.41E − 04	–	7.12E − 04	–
	40	1.88E − 05	2.98	1.04E − 04	2.93	2.25E − 05	2.64	2.49E − 04	1.52
	80	2.12E − 06	3.15	1.17E − 05	3.15	2.24E − 06	3.33	2.27E − 05	3.46
	160	2.42E − 07	3.21	1.32E − 06	3.14	2.46E − 07	3.19	1.40E − 06	4.02
p^3	20	1.96E − 05	–	3.70E − 05	–	1.93E − 05	–	3.80E − 05	–
	40	1.30E − 06	3.92	4.24E − 06	3.12	1.64E − 06	3.55	3.77E − 06	3.33
	80	7.71E − 08	4.08	1.60E − 07	4.73	8.61E − 08	4.25	1.79E − 07	4.40
	160	4.61E − 09	4.06	8.03E − 09	4.31	4.74E − 09	4.18	8.45E − 09	4.41

$\alpha = 0.5$, $\beta = \gamma = 1$, $A = c = 1$. Periodic boundary condition in $[0, 2\pi]$. Non-uniform meshes with N cells at time $t = 1$.

Table 3
Accuracy test for NLS equation (3.3) with the soliton solution (3.4)

	N	Real part				Imaginary part			
		L^2 error	Order	L^∞ error	Order	L^2 error	Order	L^∞ error	Order
p^0	80	9.22E − 02	–	7.42E − 01	–	1.00E − 01	–	7.25E − 01	–
	160	3.23E − 02	1.51	3.04E − 01	1.29	3.30E − 02	1.60	2.78E − 01	1.38
	320	1.24E − 02	1.39	1.19E − 01	1.35	1.24E − 02	1.41	1.08E − 01	1.37
	640	5.64E − 03	1.13	5.43E − 02	1.13	5.74E − 03	1.12	5.11E − 02	1.07
p^1	40	1.38E − 01	–	8.69E − 01	–	1.22E − 01	–	5.96E − 01	–
	80	2.38E − 02	2.53	1.78E − 01	2.28	2.12E − 02	2.53	1.54E − 01	1.96
	160	5.28E − 03	2.17	5.06E − 02	1.82	4.97E − 03	2.09	4.21E − 02	1.87
	320	1.25E − 03	2.08	1.31E − 02	1.95	1.16E − 03	2.10	1.07E − 02	1.98
p^2	40	1.31E − 02	–	1.07E − 01	–	1.31E − 02	–	1.25E − 01	–
	80	9.29E − 04	3.82	1.40E − 02	2.94	1.00E − 03	3.71	1.19E − 02	3.39
	160	1.04E − 04	3.15	1.84E − 03	2.93	1.01E − 04	3.30	1.84E − 03	2.70
	320	1.18E − 05	3.15	2.55E − 04	2.85	1.21E − 05	3.07	2.33E − 04	2.98
p^3	20	4.93E − 02	–	3.86E − 01	–	5.20E − 02	–	3.41E − 01	–
	40	2.62E − 03	4.24	1.75E − 02	4.46	2.36E − 03	4.46	1.80E − 02	4.25
	80	1.92E − 04	3.77	2.03E − 03	3.11	1.78E − 04	3.73	1.47E − 03	3.61
	160	1.50E − 05	3.67	1.32E − 04	3.94	1.40E − 05	3.66	1.06E − 04	3.80

Periodic boundary condition in $[-15, 15]$. Non-uniform meshes with N cells at time $t = 1$.

With such a choice of fluxes we can get the theoretical results of L^2 stability.

Proposition 2.5. (L^2 stability). *The solution to the scheme (2.24) and (2.25) satisfies the L^2 stability*

$$\frac{\mathrm{d}}{\mathrm{d}t}\int_0^L (|u|^2 + |v|^2)\mathrm{d}x \leqslant 0.$$

Proposition 2.5 can be proven by similar techniques as that in the proof of Proposition 2.1. We will thus not give the details here.

3. Numerical results

In this section we provide numerical examples to illustrate the accuracy and capability of the methods developed in the previous section. Time discretization is by the third order explicit Runge–Kutta method in [26]. We can also use the exponential time differencing fourth-order Runge–Kutta method which was developed by Cox and Matthews in [16]. We will use this efficient time discretization method in a future work.

Example 3.1. We show an accuracy test for the NLS equation

$$\mathrm{i}u_t + u_{xx} + \mathrm{i}\alpha(|u|^2 u)_x + \beta|u|^2 u + \gamma|u|^4 u = 0, \tag{3.1}$$

which admits a progressive plane wave solution

$$u(x,t) = A\exp(\mathrm{i}(cx - \omega t)), \tag{3.2}$$

where $\omega = c^2 + \alpha|A|^2 c - \beta|A|^2 - \gamma|A|^4$, A and c are constants. We use non-uniform meshes in this and later examples which are obtained by randomly perturbing each mesh point in a uniform mesh independently up

to $\pm 10\%\Delta x$. The L^2 and L^∞ errors and the numerical orders of accuracy are contained in Tables 1 and 2. We can see that the method with P^k elements gives a uniform $(k+1)$-th order of accuracy in both norms.

Example 3.2. We show an accuracy test for the NLS equation

$$iu_t + u_{xx} + 2|u|^2 u = 0, \tag{3.3}$$

with the soliton solution

$$u(x,t) = \operatorname{sech}(x - 4t)\exp\left(2i\left(cx - \frac{3}{2}t\right)\right). \tag{3.4}$$

Waves of this form play an important role in complex physical situations, for example, in coherent laser optics. It can be shown that the envelope or the modulus $|u(x,t)|$ may be considered as a soliton. The L^2

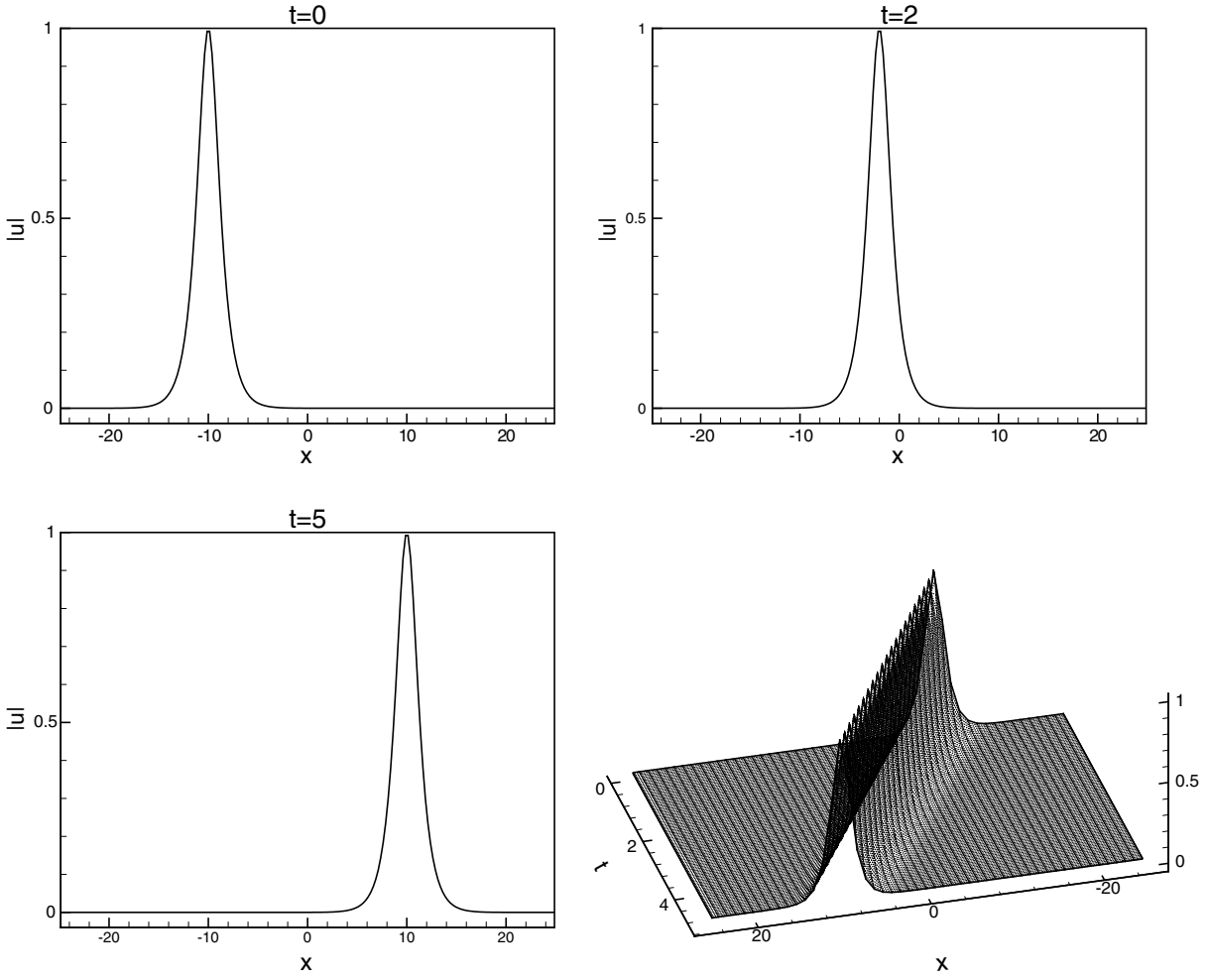

Fig. 1. The soliton propagation of Eq. (3.3) with initial condition (3.5). Periodic boundary condition in $[-25,25]$, $x_0 = -10$, P^2 elements with 200 uniform cells.

and L^∞ errors and the numerical order of accuracy are contained in Table 3. We can see that the method with P^k elements gives a uniform $(k+1)$-th order of accuracy in both norms.

Example 3.3. In this example we show the soliton propagation of Eq. (3.3) in Fig. 1 with the initial condition

$$u(x,0) = \operatorname{sech}(x - x_0)\exp(2\mathrm{i}(c(x - x_0))). \tag{3.5}$$

The double soliton collision case has the initial condition

$$u(x,0) = \sum_{j=1}^{2} \exp\left(\frac{1}{2}\mathrm{i}c_j(x - x_j)\right)\operatorname{sech}(x - x_j) \tag{3.6}$$

The solution is computed with periodic boundary condition in $[-25,25]$ using P^2 elements with 250 uniform cells and is shown in Fig. 2.

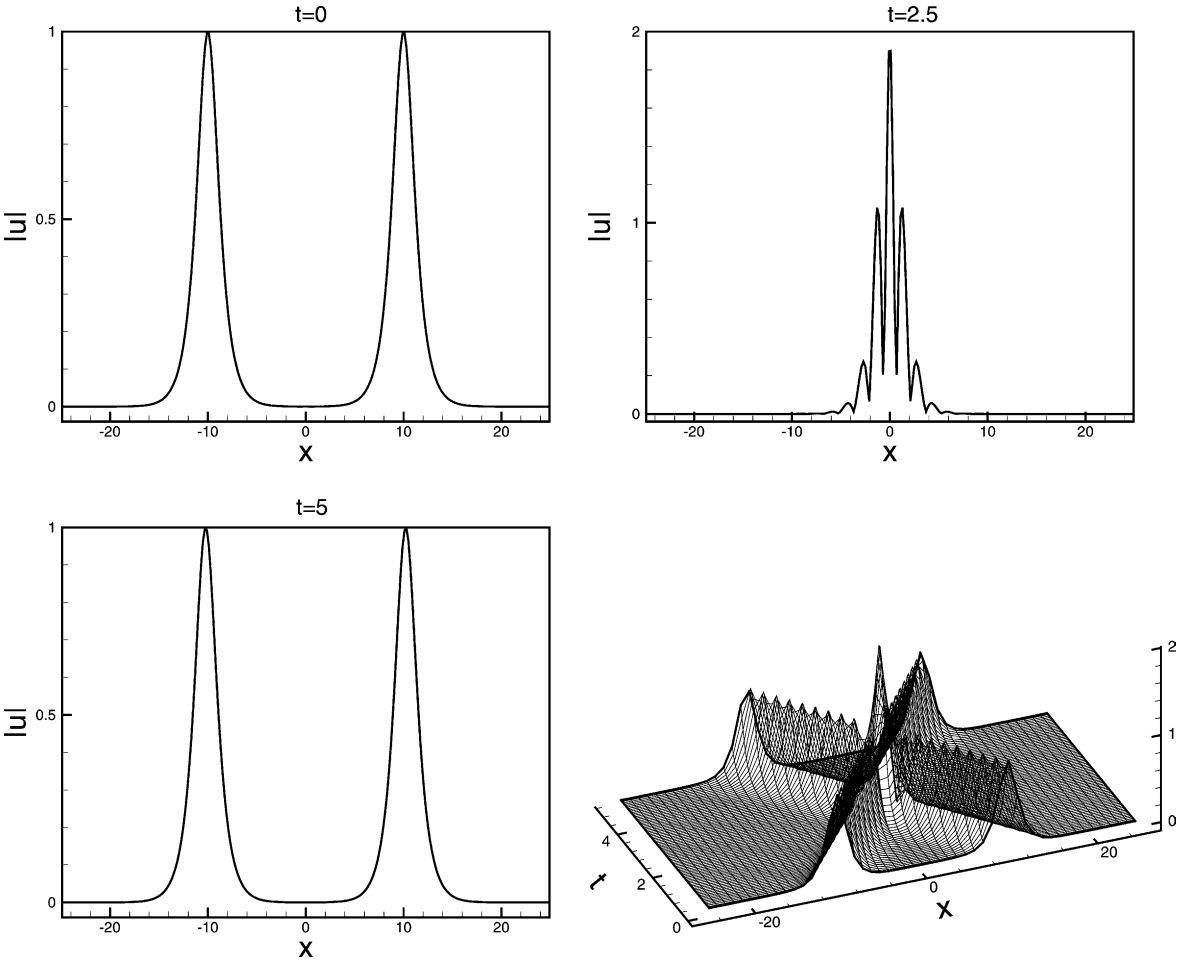

Fig. 2. The double soliton collision of Eq. (3.3) with initial condition (3.6). $c_1 = 4$, $x_1 = -10$, $c_2 = -4$, $x_2 = 10$. Periodic boundary condition in $[-25,25]$. P^2 elements with 250 uniform cells.

Example 3.4. In this example we show the birth of soliton using a square well initial condition [17]. We take the Maxwellian initial condition

$$u(x,0) = A\exp(-x^2). \tag{3.7}$$

In Fig. 3 the standing soliton is observed.

A second simulation involves the initial condition

$$u(x,0) = A\exp(-x^2 + 2\mathrm{i}x). \tag{3.8}$$

In Fig. 4 the mobile soliton is observed.

Example 3.5. In this example we show the bound state solution of the equation

$$\mathrm{i}u_t + u_{xx} + \beta|u|^2 u = 0, \tag{3.9}$$

with the initial condition

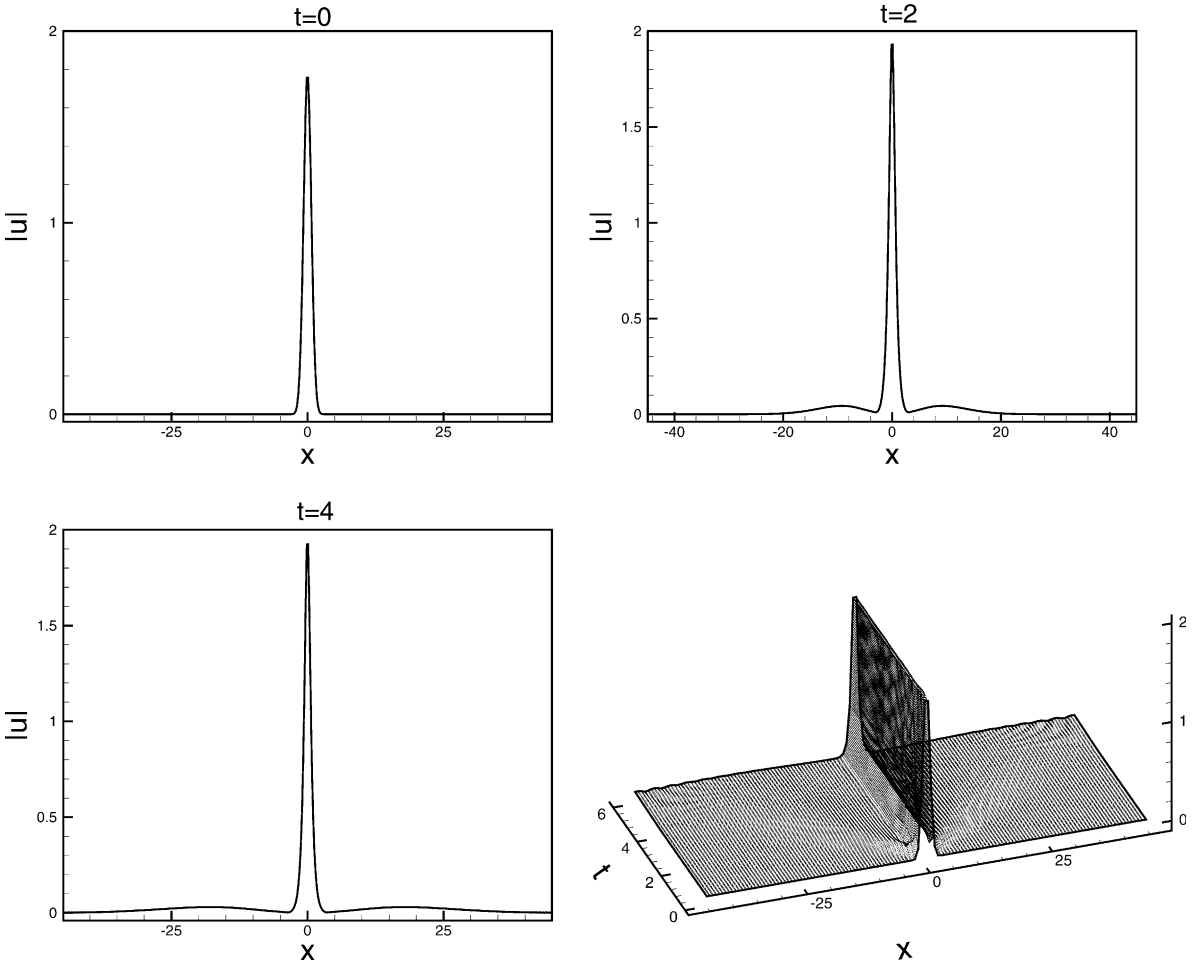

Fig. 3. The birth of standing soliton of Eq. (3.3) with initial condition (3.7). $A = 1.78$. Periodic boundary condition in $[-45,45]$. P^2 elements with 400 uniform cells.

$$u(x,0) = \operatorname{sech} x. \tag{3.10}$$

It will produce a bound state of N solitons if

$$\beta = 2N^2. \tag{3.11}$$

The theoretical solution for a bound state of solitons is known [23]. The solutions develop small narrow structure which are difficult to resolve if $N \geqslant 3$. In Figs. 5–7, we show the numerical approximation of the bound state of soliton for $N = 3, 4, 5$.

Example 3.6. We show an accuracy test for the coupled NLS equation

$$\begin{cases} \mathrm{i}u_t + \mathrm{i}\alpha u_x + \frac{1}{2}u_{xx} + (|u|^2 + \beta|v|^2)u = 0, \\ \mathrm{i}v_t - \mathrm{i}\alpha v_x + \frac{1}{2}v_{xx} + (\beta|u|^2 + |v|^2)v = 0, \end{cases} \tag{3.12}$$

with the soliton solution

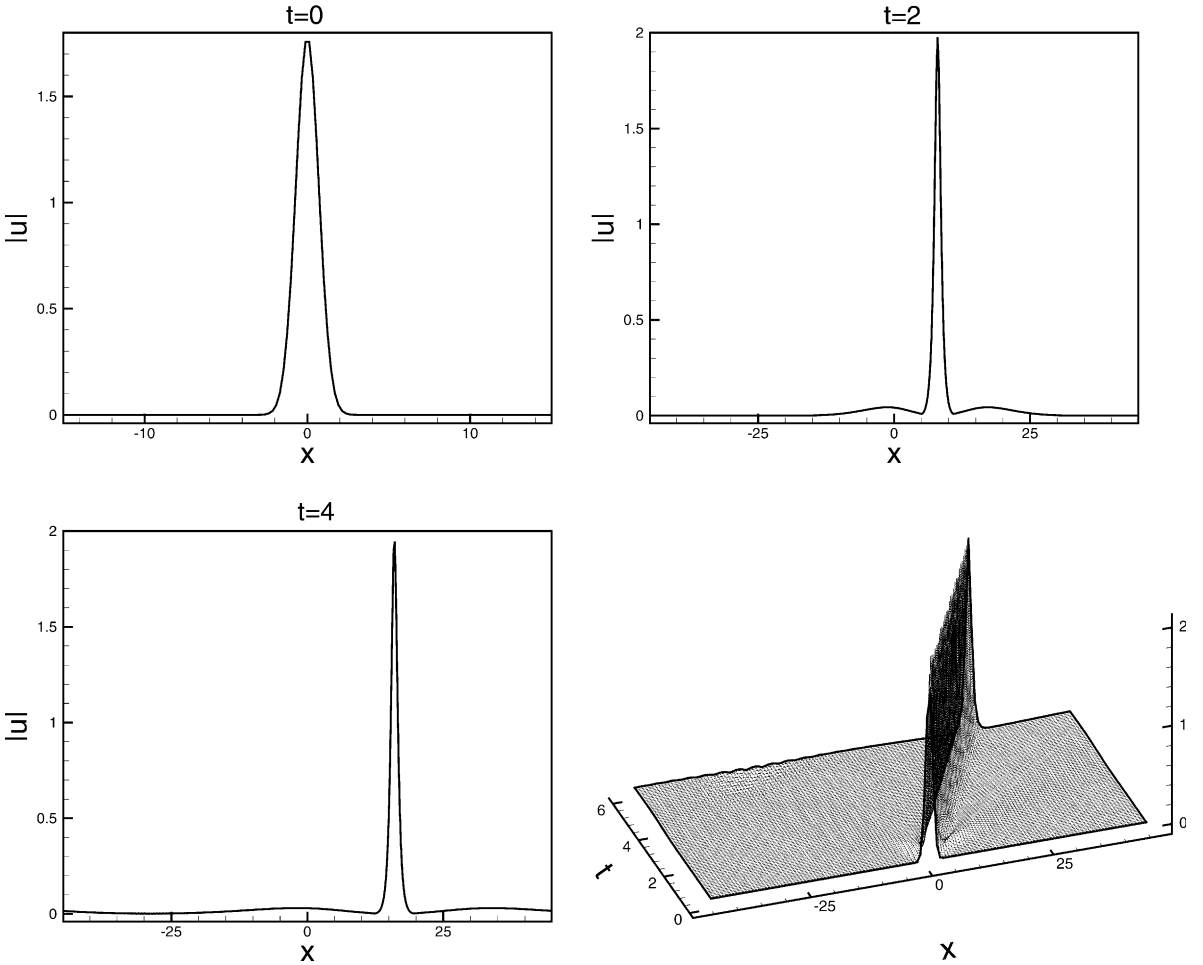

Fig. 4. The birth of mobile soliton of Eq. (3.3) with initial condition (3.8). $A = 1.78$. Periodic boundary condition in $[-45, 45]$. P^2 elements with 400 uniform cells.

$$
\begin{aligned}
u(x,t) &= \sqrt{\frac{2a}{1+\beta}}\operatorname{sech}(\sqrt{2a}(x-ct))\exp\left(\mathrm{i}\left((c-\alpha)x-\left(\frac{c^2-\alpha^2}{2}-a\right)t\right)\right),\\
v(x,t) &= \sqrt{\frac{2a}{1+\beta}}\operatorname{sech}(\sqrt{2a}(x-ct))\exp\left(\mathrm{i}\left((c+\alpha)x-\left(\frac{c^2-\alpha^2}{2}-a\right)t\right)\right),
\end{aligned}
\tag{3.13}
$$

The L^2 and L^∞ errors and the numerical order of accuracy are contained in Table 4. We can see that the method with P^k elements gives a uniform $(k+1)$-th order of accuracy in both norms.

We also present the solitary wave propagation for the coupled NLS equation (3.12) in Fig. 8 with the initial condition

$$
\begin{aligned}
u(x,0) &= \sqrt{\frac{2a}{1+\beta}}\operatorname{sech}(\sqrt{2a}(x-x_0))\exp(\mathrm{i}((c-\alpha)(x-x_0))),\\
v(x,0) &= \sqrt{\frac{2a}{1+\beta}}\operatorname{sech}(\sqrt{2a}(x-x_0))\exp(\mathrm{i}((c+\alpha)(x-x_0))).
\end{aligned}
\tag{3.14}
$$

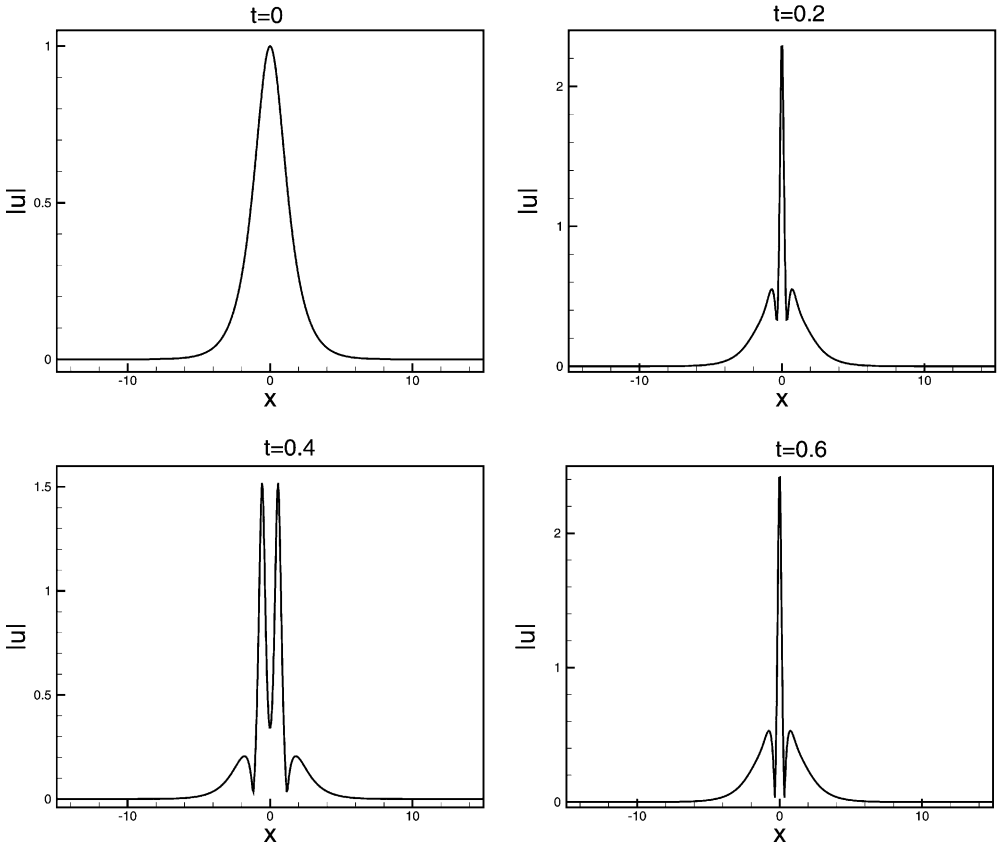

Fig. 5. The bound state solution of Eq. (3.9) with initial condition (3.10). $N = 3$. Periodic boundary condition in $[-15, 15]$. P^2 elements with 500 uniform cells.

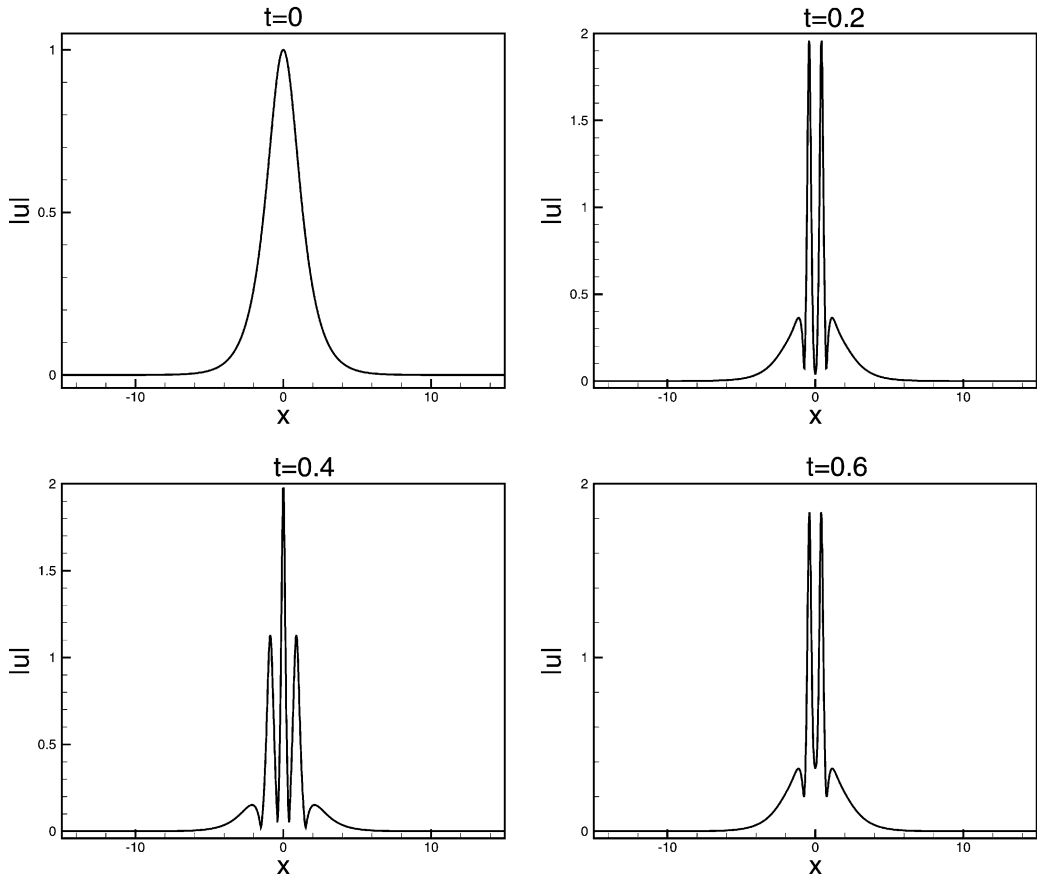

Fig. 6. The bound state solution of Eq. (3.9) with initial condition (3.10). $N = 4$. Periodic boundary condition in $[-15, 15]$. P^2 elements with 800 uniform cells.

Example 3.7. In this example we show the soliton interaction for the coupled NLS equation (3.12). The double soliton collision case has the initial condition

$$\begin{aligned} u(x,0) &= \sum_{j=1}^{2} \sqrt{\frac{2a_j}{1+\beta}} \operatorname{sech}(\sqrt{2a_j}(x-x_j)) \exp(\mathrm{i}((c_j-\alpha)(x-x_j))), \\ v(x,0) &= \sum_{j=1}^{2} \sqrt{\frac{2a_j}{1+\beta}} \operatorname{sech}(\sqrt{2a_j}(x-x_j)) \exp(\mathrm{i}((c_j+\alpha)(x-x_j))), \end{aligned} \tag{3.15}$$

where $\alpha = 0.5$, $\beta = 2/3$, $c_1 = 1$, $c_2 = 0.1$, $a_1 = 1$, $a_2 = 0.5$, $x_1 = 0$, $x_2 = 25$. The solution is computed with periodic boundary condition in $[-20, 80]$. P^2 elements with 400 cells are used and the result is shown in Fig. 9.

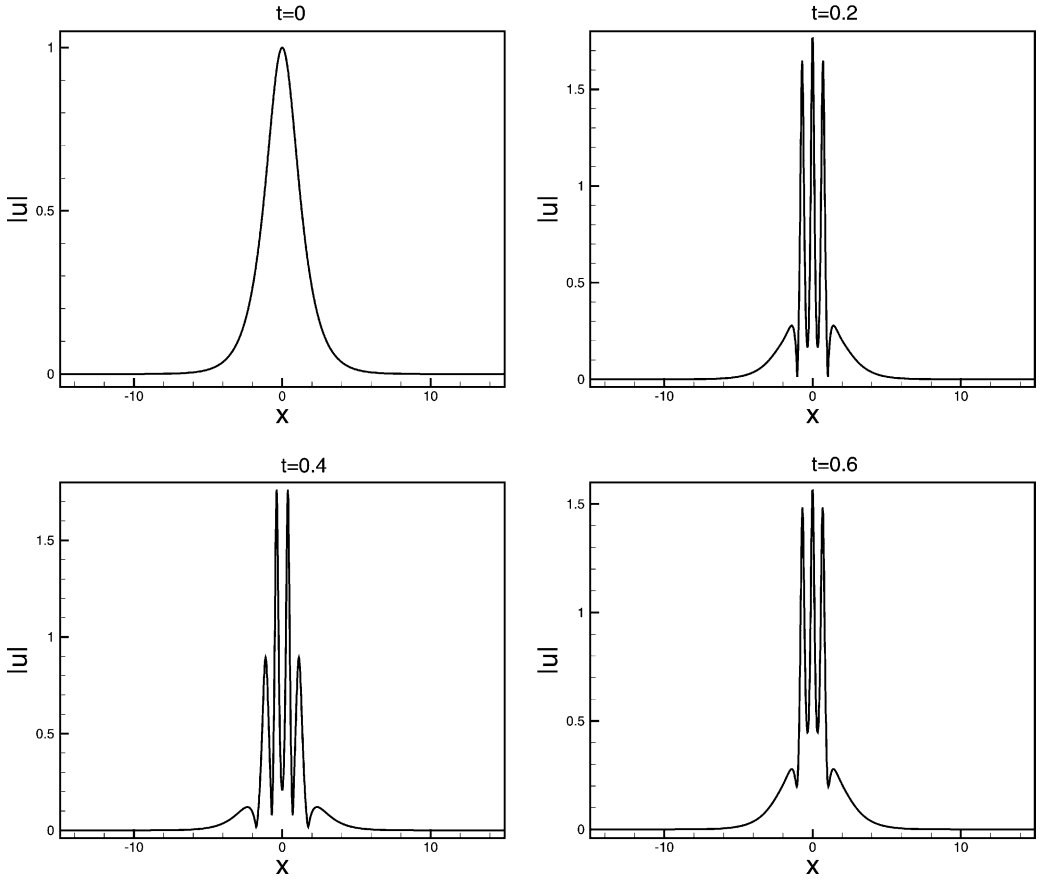

Fig. 7. The bound state solution of Eq. (3.9) with initial condition (3.10). $N = 5$. Periodic boundary condition in $[-15, 15]$. P^2 elements with 1000 uniform cells.

The triple soliton collision case has the initial condition

$$\begin{aligned} u(x,0) &= \sum_{j=1}^{3} \sqrt{\frac{2a_j}{1+\beta}} \operatorname{sech}(\sqrt{2a_j}(x-x_j)) \exp(\mathrm{i}((c_j-\alpha)(x-x_j))), \\ v(x,0) &= \sum_{j=1}^{3} \sqrt{\frac{2a_j}{1+\beta}} \operatorname{sech}(\sqrt{2a_j}(x-x_j)) \exp(\mathrm{i}((c_j+\alpha)(x-x_j))), \end{aligned} \tag{3.16}$$

where $\alpha = 0.5$, $\beta = 2/3$, $c_1 = 1$, $c_2 = 0.1$, $c_3 = -1$, $a_1 = 1$, $a_2 = 0.72$, $a_3 = 0.36$, $x_1 = 0$, $x_2 = 25$, $x_3 = 50$. The solution is computed with periodic boundary condition in $[-20, 80]$. P^2 elements with 400 cells are used and the result is shown in Fig. 10.

Example 3.8. We show an accuracy test for the two-dimensional NLS equation

$$\mathrm{i}u_t + u_{xx} + u_{yy} + \beta|u|^2 u = 0, \tag{3.17}$$

which admits a progressive plane wave solution

$$u(x,t) = A \exp(\mathrm{i}(c_1 x + c_2 y - \omega t)), \tag{3.18}$$

Table 4
Accuracy test for the coupled NLS equation (3.12) with the soliton solution (3.13)

	N	Real part of u				Imaginary part of u			
		L^2 error	Order	L^∞ error	Order	L^2 error	Order	L^∞ error	Order
p^0	80	1.76E − 01	–	2.99E − 01	–	2.37E − 01	–	4.49E − 01	–
	160	1.16E − 01	0.60	2.13E − 01	0.49	1.34E − 01	0.82	2.48E − 01	0.86
	320	7.05E − 02	0.72	1.31E − 01	0.70	7.69E − 02	0.80	1.40E − 01	0.82
	640	3.99E − 02	0.82	7.43E − 02	0.82	4.14E − 02	0.89	7.56E − 02	0.89
p^1	80	6.72E − 02	–	1.18E − 01	–	7.36E − 02	–	2.66E − 01	–
	160	1.82E − 02	1.89	3.33E − 02	1.83	1.54E − 02	2.26	6.49E − 02	2.03
	320	4.47E − 03	2.03	8.11E − 03	2.04	3.69E − 03	2.06	1.54E − 02	2.07
	640	1.21E − 03	1.88	2.18E − 03	1.89	9.83E − 04	1.91	4.04E − 03	1.93
p^2	80	6.91E − 03	–	1.91E − 02	–	6.38E − 03	–	2.17E − 02	–
	160	5.48E − 04	3.66	2.18E − 03	3.13	6.18E − 04	3.37	2.50E − 03	3.12
	320	5.19E − 05	3.40	3.05E − 04	2.84	6.76E − 05	3.19	3.52E − 04	2.82
	640	5.34E − 06	3.28	3.19E − 05	3.26	8.04E − 06	3.07	5.21E − 05	2.76
p^3	80	2.03E − 03	–	3.51E − 03	–	1.44E − 03	–	4.21E − 03	–
	160	1.23E − 04	4.04	2.49E − 04	3.82	1.02E − 04	3.82	5.01E − 04	3.07
	320	9.51E − 06	3.69	1.78E − 05	3.81	7.08E − 06	3.85	3.16E − 05	3.99
	640	5.91E − 07	4.01	1.30E − 06	3.77	4.34E − 07	4.03	1.99E − 06	3.99
p^0	80	3.60E − 01	–	7.52E − 01	–	2.58E − 01	–	4.57E − 01	–
	160	2.27E − 01	0.67	4.85E − 01	0.63	1.71E − 01	0.59	3.11E − 01	0.55
	320	1.33E − 01	0.78	2.87E − 01	0.76	9.76E − 02	0.81	2.07E − 01	0.59
	640	7.34E − 02	0.85	1.63E − 01	0.81	5.24E − 02	0.90	1.20E − 01	0.79
p^1	80	1.11E − 01	–	3.00E − 01	–	8.40E − 02	–	2.16E − 01	–
	160	2.91E − 02	1.98	1.01E − 01	1.57	2.11E − 02	2.00	7.50E − 02	1.53
	320	6.99E − 03	2.01	2.66E − 02	1.93	5.12E − 03	2.04	1.77E − 02	2.08
	640	1.86E − 03	1.91	6.27E − 03	2.08	1.37E − 03	1.90	5.55E − 03	1.68
p^2	80	1.15E − 02	–	3.36E − 02	–	1.26E − 02	–	5.04E − 02	–
	160	1.33E − 03	3.11	7.15E − 03	2.23	1.22E − 03	3.36	5.65E − 03	3.16
	320	1.47E − 04	3.18	8.02E − 04	3.16	1.53E − 04	3.00	8.76E − 04	2.69
	640	1.79E − 05	3.03	1.26E − 04	2.67	1.76E − 05	3.12	9.60	3.19
p^3	80	3.01E − 03	–	5.07E − 03	–	2.37E − 03	–	7.24E − 03	–
	160	2.18E − 04	3.79	9.75E − 04	2.38	1.83E − 04	3.70	4.67E − 04	3.95
	320	1.49E − 05	3.86	6.05E − 05	4.01	1.20E − 05	3.93	4.49E − 05	3.38
	640	9.17E − 07	4.03	3.28E − 06	4.20	7.42E − 07	4.01	3.21E − 06	3.80

$c = 1$, $\alpha = 0.5$, $a = 1$, $\beta = 2/3$. Periodic boundary condition in $[-25, 25]$. Non-uniform meshes with N cells at time $t = 1$.

where $\omega = c_1^2 + c_2^2 - \beta|A|^2$, A, c_1 and c_2 are constants. We use uniform and non-uniform rectangular meshes, the non-uniform meshes have independent random perturbations in each of the x and y directions. The L^2 and L^∞ errors and the numerical order of accuracy are contained in Table 5. We can see that the method with P^k elements gives a uniform $(k + 1)$-th order of accuracy in both norms.

Example 3.9. In this example we show singular solutions for the two-dimensional NLS equation

$$\mathrm{i}u_t + u_{xx} + u_{yy} + |u|^2 u = 0. \tag{3.19}$$

We choose the initial condition

$$u(x, y) = (1 + \sin x)(2 + \sin y) \tag{3.20}$$

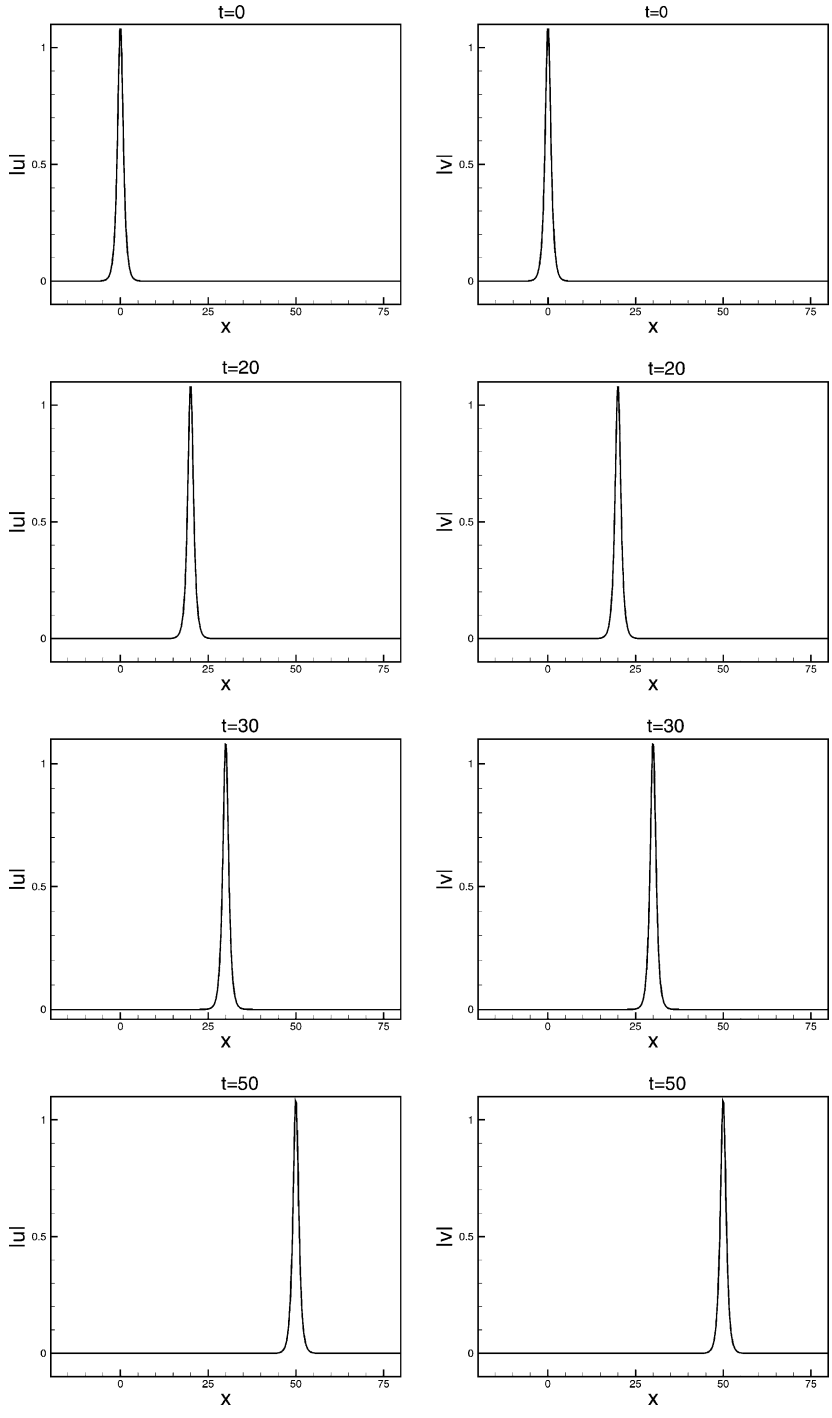

Fig. 8. The solitary wave propagation of Eq. (3.12) with initial condition (3.14). $\alpha = 0.5$, $\beta = 2/3$, $c = 1$, $a = 1$, $x_0 = 0$. Periodic boundary condition in $[-20, 80]$. P^2 elements with 400 uniform cells.

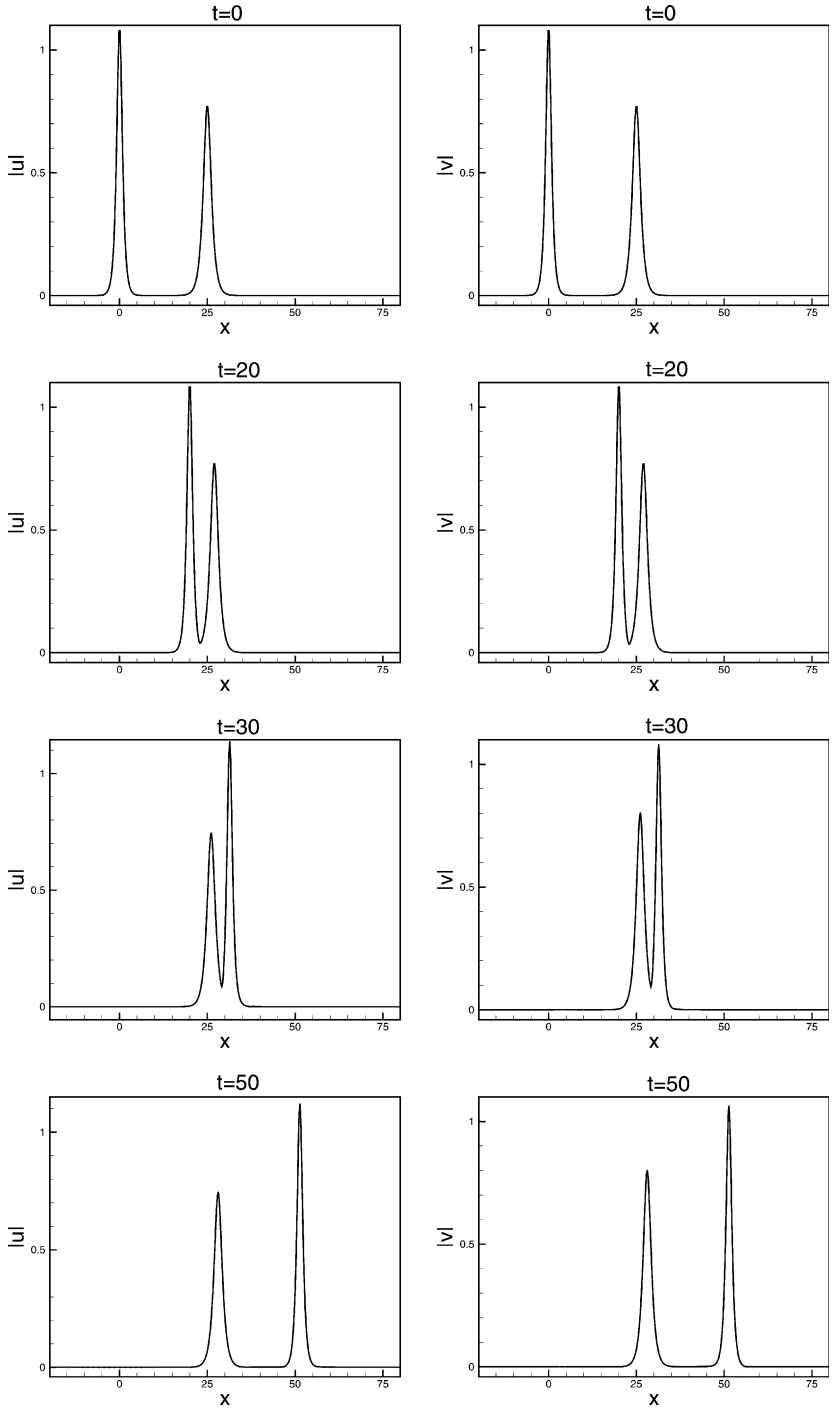

Fig. 9. The double soliton collision of Eq. (3.12) with initial condition (3.15). $\alpha = 0.5$, $\beta = 2/3$, $c_1 = 1$, $c_2 = 0.1$, $a_1 = 1$, $a_2 = 0.5$, $x_1 = 0$, $x_2 = 25$. Periodic boundary condition in $[-20, 80]$. P^2 elements with 400 uniform cells.

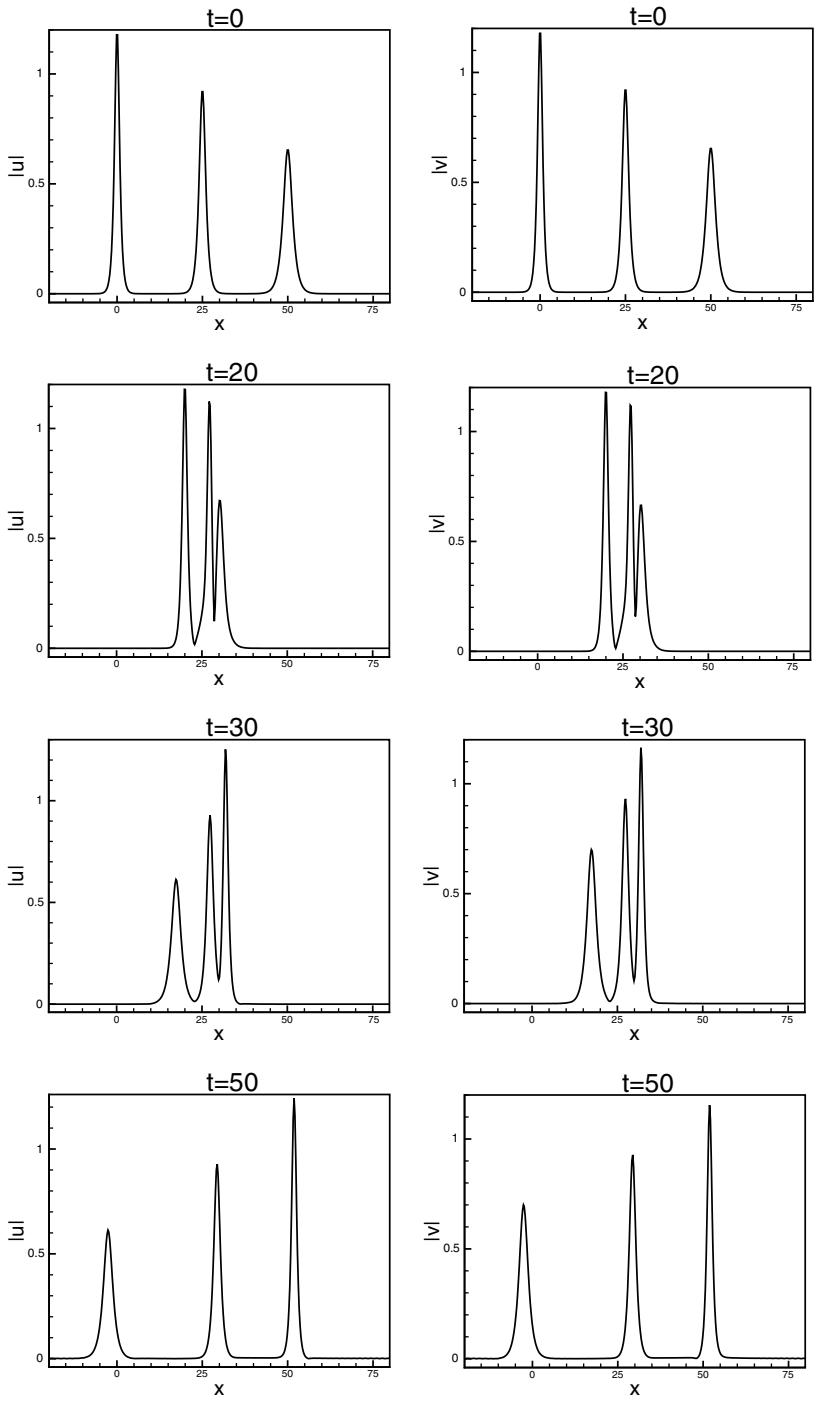

Fig. 10. The triple soliton collision of Eq. (3.12) with initial condition (3.16). $\alpha = 0.5$, $\beta = 2/3$, $c_1 = 1$, $c_2 = 0.1$, $c_3 = -1$, $a_1 = 1$, $a_2 = 0.72$, $a_3 = 0.36$, $x_1 = 0$, $x_2 = 25$, $x_3 = 50$. Periodic boundary condition in $[-20, 80]$. P^2 elements with 400 uniform cells.

Table 5
Accuracy test for the NLS equation (3.17) with the plane solution (3.18)

	$N \times N$	Real part				Imaginary part			
		L^2 error	Order	L^∞ error	Order	L^2 error	Order	L^∞ error	Order
p^0	10×10	2.30E − 01	–	1.08	–	2.16E − 01	–	7.57E − 01	–
	20×20	1.05E − 01	1.13	4.72E − 01	1.20	1.05E − 01	1.03	4.72E − 01	0.68
	40×40	4.91E − 02	1.10	2.30E − 01	1.04	4.92E − 02	1.10	2.30E − 01	1.04
	80×80	2.42E − 02	1.02	1.22E − 01	0.92	2.42E − 02	1.02	1.21E − 01	0.92
p^1	10×10	1.24E − 01	–	3.43E − 01	–	2.81E − 02	–	9.88E − 02	–
	20×20	2.82E − 02	2.13	9.87E − 02	1.60	2.82E − 02	2.13	9.43E − 02	1.87
	40×40	6.70E − 03	2.07	2.50E − 02	1.98	6.71E − 03	2.07	2.45E − 02	1.95
	80×80	1.64E − 03	2.03	5.93E − 03	2.08	1.64E − 03	2.03	6.04E − 03	2.02
p^2	10×10	7.12E − 03	–	5.69E − 02	–	6.95E − 03	–	5.76E − 02	–
	20×20	6.83E − 04	3.38	6.89E − 03	3.04	7.15E − 04	3.28	7.01E − 03	3.04
	40×40	7.96E − 05	3.10	8.75E − 04	2.98	7.99E − 05	3.16	9.52E − 04	2.88
	80×80	9.11E − 06	3.13	1.02E − 04	3.11	9.10E − 06	3.13	1.04E − 04	3.19
p^3	10×10	1.48E − 03	–	8.40E − 03	–	1.45E − 03	–	7.19E − 03	–
	20×20	9.16E − 05	4.02	6.01E − 04	3.81	9.23E − 05	3.97	5.41E − 04	3.73
	40×40	5.66E − 06	4.02	4.72E − 05	3.67	5.64E − 06	4.03	3.18E − 05	4.09
	80×80	3.53E − 07	4.00	2.14E − 06	4.47	3.52E − 07	4.00	2.33E − 06	3.77

$\beta = 2$, $A = c = 1$. Periodic boundary condition in $[0, 2\pi]$. Non-uniform meshes with $N \times N$ cells at time $t = 1$.

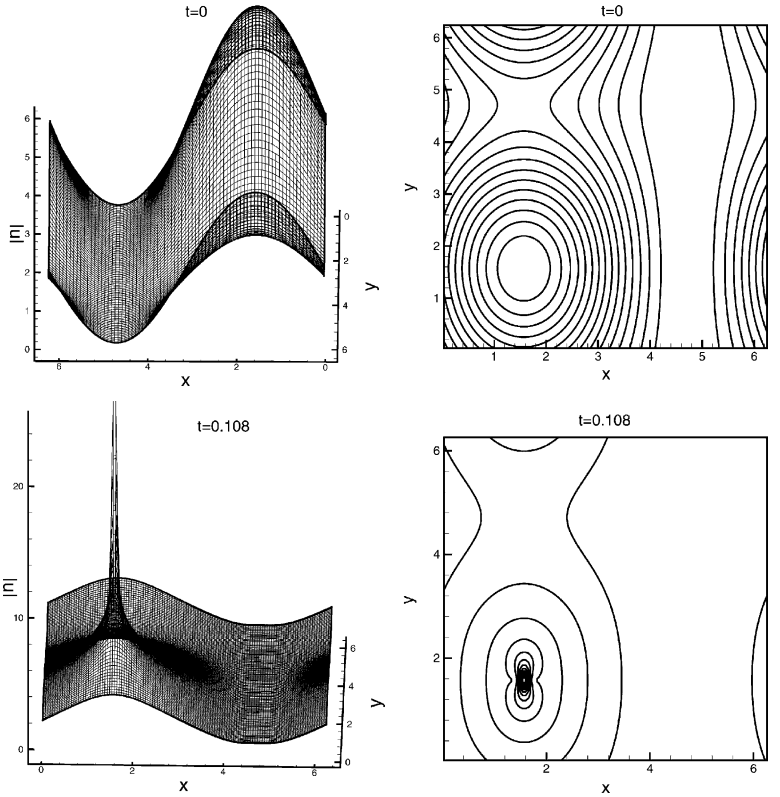

Fig. 11. The singular solution of Eq. (3.19) with initial condition (3.20). Periodic boundary condition in $[0, 2\pi]$. P^2 elements with 120×120 uniform cells.

and a periodic boundary condition. Strong evidence of a singularity in finite time is obtained, although there is no rigorous proof of breakdown in this case [27]. The solution is computed with a periodic boundary condition in $[0, 2\pi]$ using P^2 elements with 120×120 uniform cells. The result is shown in Fig. 11.

4. Concluding remarks

We have developed the local discontinuous Galerkin methods to solve generalized nonlinear Schrödinger equations, including coupled Schrödinger equations and two-dimensional Schrödinger equations, and have proven the stability of these methods. Numerical examples for nonlinear problems are shown to illustrate the accuracy and capability of the methods. Although not addressed in this paper, these methods are flexible for general geometry, unstructured meshes and h–p adaptivity, and have excellent parallel efficiency. They should provide a useful class of numerical tools for solving the nonlinear Schrödinger equations.

Acknowledgments

This research was partially supported by the Chinese Academy of Sciences while the second author was in residence at the University of Science and Technology of China (Grant 2004-1-8) and at the Institute of Computational Mathematics and Scientific/Engineering Computing. Additional support is provided by ARO Grants DAAD19-00-1-0405 and W911NF-04-1-0291, NSF Grant DMS-0207451 and AFOSR Grant F49620-02-1-0113.

References

[1] F. Bassi, S. Rebay, A high-order accurate discontinuous finite element method for the numerical solution of the compressible Navier–Stokes equations, J. Comput. Phys. 131 (1997) 267–279.
[2] D.J. Benney, A.C. Newll, The propagation of nonlinear wave envelops, J. Math. Phys. 46 (1967) 133–139.
[3] I. Białynicki-Birula, J. Mycielski, Gaussons: solitons of the logarithmic Schrödinger equation, Phys. Scripta 20 (1979) 539–544.
[4] R.K. Bullough, P.M. Jack, P.W. Kitchenside, R. Saunders, Solitons in laser physics, Phys. Scripta 20 (1979) 364–381.
[5] Q.S. Chang, E. Jia, W. Sun, Difference schemes for solving the generalized nonlinear Schrödinger equation, J. Comput. Phys. 148 (1999) 397–415.
[6] P. Ciarlet, The finite element method for elliptic problem, North-Holland, Amsterdam, 1975.
[7] B. Cockburn, Discontinuous Galerkin methods for methods for convection-dominated problems, in: T.J. Barth, H. Deconinck (Eds.), High-Order Methods for Computational Physics, Lecture Notes in Computational Science and Engineering, vol. 9, Springer, Berlin, 1999, pp. 69–224.
[8] B. Cockburn, S. Hou, C.-W. Shu, The Runge–Kutta local projection discontinuous Galerkin finite element method for conservation laws IV: the multidimensional case, Math. Comput. 54 (1990) 545–581.
[9] B. Cockburn, G. Karniadakis, C.-W. Shu, The development of discontinuous Galerkin methods, in: B. Cockburn, G. Karniadakis, C.-W. Shu (Eds.), Lecture Notes in Computational Science and Engineering, vol. 11, Springer, Berlin, 2000, pp. 3–50, Part I: Overview.
[10] B. Cockburn, S.-Y. Lin, C.-W. Shu, TVB Runge–Kutta local projection discontinuous Galerkin finite element method for conservation laws III: one dimensional systems, J. Comput. Phys. 84 (1989) 90–113.
[11] B. Cockburn, C.-W. Shu, TVB Runge–Kutta local projection discontinuous Galerkin finite element method for conservation laws II: general framework, Math. Comput. 52 (1989) 411–435.
[12] B. Cockburn, C.-W. Shu, The Runge–Kutta discontinuous Galerkin method for conservation laws V: multidimensional systems, J. Comput. Phys. 141 (1998) 199–224.
[13] B. Cockburn, C.-W. Shu, The local discontinuous Galerkin method for time-dependent convection–diffusion systems, SIAM J. Numer. Anal. 35 (1998) 2440–2463.

[14] B. Cockburn, C.-W. Shu, Runge–Kutta discontinuous Galerkin methods for convection-dominated problems, J. Sci. Comput. 16 (2001) 173–261.
[15] S. Cowan, R.H. Enns, S.S. Rangnekar, S.S. Sanghera, Quasi-soliton and other behaviour of the nonlinear cubic-quintic Schrödinger equation, Can. J. Phys. 64 (1986) 311–315.
[16] S.M. Cox, P.C. Matthews, Exponential time differencing for stiff systems, J. Comput. Phys. 176 (2002) 430–455.
[17] I. Dağ, A quadratic B-spline finite element method for solving nonlinear Schrödinger equation, Comput. Methods Appl. Mech. Eng. 174 (1999) 247–258.
[18] R.T. Glassey, On the blowing up of solutions to the Cauchy problem for nonlinear Schrödinger equations, J. Math. Phys. 18 (1977) 1794–1797.
[19] M.S. Ismail, T.R. Taha, Numerical simulation of coupled nonlinear Schrödinger equation, Math. Comput. Simulation 56 (2001) 547–562.
[20] O. Karakashian, C. Makridakis, A space–time finite element method for the nonlinear Schrödinger equation: the discontinuous Galerkin method, Math. Comput. 67 (1998) 479–499.
[21] O. Karakashian, C. Makridakis, A space–time finite element method for the nonlinear Schrödinger equation: the continuous Galerkin method, SIAM J. Numer. Anal. 36 (1999) 1779–1807.
[22] D. Levy, C.-W. Shu, J. Yan, Local discontinuous Galerkin methods for nonlinear dispersive equations, J. Comput. Phys. 196 (2004) 751–772.
[23] J.W. Miles, An envelope soliton problem, SIAM J. Appl. Math. 41 (1981) 227–230.
[24] D. Pathria, J.L. Morris, Pseudo-spectral solution of nonlinear Schrödinger equations, J. Comput. Phys. 87 (1990) 108–125.
[25] Q. Sheng, A.Q.M. Khaliq, E.A. Al-Said, Solving the generalized nonlinear Schrödinger equation via quartic spline approximation, J. Comput. Phys. 166 (2001) 400–417.
[26] C.-W. Shu, S. Osher, Efficient implementation of essentially non-oscillatory shock-capturing schemes, J. Comput. Phys. 77 (1988) 439–471.
[27] P.L. Sulem, C. Sulem, A. Patera, Numerical simulation of singular solutions to the two-dimensional cubic Schrödinger equation, Commun. Pure Appl. Math. 37 (1984) 755–778.
[28] J.Q. Sun, M.Z. Qin, Multi-symplectic methods for the coupled 1D nonlinear Schrödinger system, Comput. Phys. Commun. 155 (2003) 221–235.
[29] T.R. Taha, M.J. Ablowitz, Analytical and numerical aspects of certain nonlinear evolution equations II. Numerical, nonlinear Schrödinger equation, J. Comput. Phys. 55 (1984) 203–230.
[30] Y. Xu, C.-W. Shu, Local discontinuous Galerkin methods for three classes of nonlinear wave equations, J. Comput. Math. 22 (2004) 250–274.
[31] J. Yan, C.-W. Shu, A local discontinuous Galerkin method for KdV type equations, SIAM J. Numer. Anal. 40 (2002) 769–791.
[32] J. Yan, C.-W. Shu, Local discontinuous Galerkin methods for partial differential equations with higher order derivatives, J. Sci. Comput. 17 (2002) 27–47.
[33] J.K. Yang, Classification of the solitary waves in coupled nonlinear Schrödinger equations, Physica D 108 (1997) 92–112.
[34] V.E. Zakharov, V.S. Synakh, The nature of self-focusing singularity, Sov. Phys. JETP 41 (1975) 465–468.